# Stability Analysis of Underground Cavity by Numerical Modeling

by

Songwen Deng

Submitted in partial fulfilment of the requirements
for the degree of Master of Applied Science

at

Dalhousie University
Halifax, Nova Scotia
June 2024

# Table of Contents

# LIST OF TABLES

# LIST OF FIGURES

# ABSTRACT

Ground subsidence is of great concern around the world. This thesis investigates the stability above and around an assumed underground cavity in cohesive soil and limestone through numerical modeling conducted with Examine 2D and Phase 2 (RS2). Strength factor (S.F.) were observed and used to assess the stability for different materials and water conditions. The analyzed area is considered unstable if the S.F. is lower than 1.

Two primary scenarios have been evaluated: 'Fixed bottom' and 'Fixed dimension', which focus on the stability impact of different overburden thicknesses and cavity dimensions. The research aims to provide insight into the factors affecting stability above and around underground voids, considering both dry and fully saturated conditions.

The study demonstrates that the stability of the ground surface correlates with the overburden thickness. If the unstable zone around the void intersects with the ground surface, then the surface will collapse.

For cohesive soil, consistencies defined by cohesion and friction angle were critical. a thicker overburden thickness was necessary for stability for lower cohesion, especially under saturated conditions. Because the presence of water further reduced material strength due to increased pore water pressure. For a 9-meter-wide horseshoe-shaped cavity with bottom fixed at 50 meters depth, the minimum overburden thickness to achieve the stability of the ground surface decreases from 22 meters to 16 meters under fully saturated conditions and 18 meters to 16 meters under dry conditions, as the cohesion increases from 18 kPa to 72 kPa. For a 9-meter-wide and 10-meter-height horseshoe-shaped cavity at varying elevations, the minimum required overburden thickness decreases from 8 meters to 2 meters under fully saturated conditions and 4 meters to 2 meters under dry conditions, as the cohesion increases from 18 kPa to 72 kPa.

Similar trends were observed in limestone, where the Geological Strength Index (GSI) has great impact on the stability. Higher GSI values correspond to increased stability of the overburden. For the same fixed-bottom cavity, the minimum required overburden thickness to achieve the stability of the ground surface decreases from 16 meters to 2 meters under fully saturated conditions and 14 meters to 2 meters under dry conditions, as the GSI value increases from 10 to 50. For the same fixed-dimension cavity at varying elevations, the minimum overburden thickness decreases from 2 meters to 1 meter under fully saturated conditions and maintains at 1 meter under dry conditions, , as the GSI value increases from 10 to 30.

The weak zones around cavities were also examined. Results showed that weaker materials and saturated conditions lead to larger unstable zones around the cavity, which might become the route for the growth of sinkholes.

# LIST OF ABBREVIATIONS AND SYMBOLS USED

| | |
|---|---|
| c | Cohesion |
| D | Disturbance factor |
| m | Meter |
| $m^2$ | Square meters |
| GSI | Geological strength index |
| $H_o$ | Void height |
| H | Thickness of overburden |
| $H_1$ | Safe zone depth |
| $H_2$ | Maximum weak zone height |
| $H_m$ | Minimum overburden thickness to maintain stability of ground surface |
| HU | The HU value for the material, a factor between 0 and 1, by which the vertical distance from a point (in soil or rock) to a water surface is multiplied to obtain the pressure head |
| $K_o$ | Horizontal stress ratio (also known as Coefficient of Earth Pressure at Rest) |
| kPa | Kilopascal |
| $m_i$ | Intact rock constant |
| $MN/m^3$ | Meganewton per cubic meter |
| MPa | Megapascal |
| $q_u$ | Unconfined compressive strength |

| | |
|---|---|
| $W_o$ | Void width |
| RS2 | Phase 2 (Rock and Soil 2-dimensional analysis program) |
| S.F. | Strength factor |
| Ψ | Friction angle |
| ° | Degree sign |

# ACKNOWLEDGEMENTS

I would like to express my deepest gratitude to my supervisor, Dr. Steve Zou for giving me the opportunity to pursue graduate studies in Canada. His expertise, knowledge, understanding, and patience enhanced my graduate experience. I appreciate his guidance and support throughout this journey.

I would also like to thank Dr. Cui Lin for being my co- supervisor and providing valuable feedback, insightful comments and encouragement. I appreciated every support she provided during the research work, as well as Dr. Hany El Naggar and Dr. Lei Liu for being my committee members and offering valuable comments to the thesis.

Finally, I wish to express my grateful to my mom, who has always believed in me and supported me in all my endeavors. Without her unwavering support and encouragement, I could not have made it this far.

Thank you all.

# Chapter 1 Introduction

## 1.1 Research background

### 1.1.1 Surface subsidence

Surface subsidence is regarded as a problem in many countries, it refers to a surface point sinking to a lower level and can include a structure settling into the ground or the ground itself lowering and carrying the structure with it, or even a surface layer collapsing into an underground cavity, which could be a natural sinkhole or an underground mine working.

The physical properties of the overburden materials (soil and bedrock) influence their settlement behavior, particularly their consolidation characteristics in relation to the conditions and magnitude of loading (Reddish & Whittaker, 2012).

### 1.1.2 Natural sinkhole

Sinkholes are depressions or shafts formed at a soil surface due to changes in the soil and/or rock beneath. In limestone areas, the gradual solution of rock at a depth through the passage of groundwater leads to subsidence of the overburden of residual and deposited soil and a resulting saucer-shaped region, often known as a solution depression (Sowers, 1996). Limestone (or karst) areas in Florida (Ruth et al., 1985; Wilson, 1995) provide many examples of geologically generated sinkholes. Of greater concern to the engineers is the sinkholes formed from the collapse of an underground cavity. These often start as small cavities. At some point, the cavity becomes sufficiently large that the remaining overburden is no longer able to arch across the cavity and collapses (Augarde

et al., 2003). Figure 1.1 illustrates the principal physical features of natural sinkhole and crown hole development in limestone rock formations.

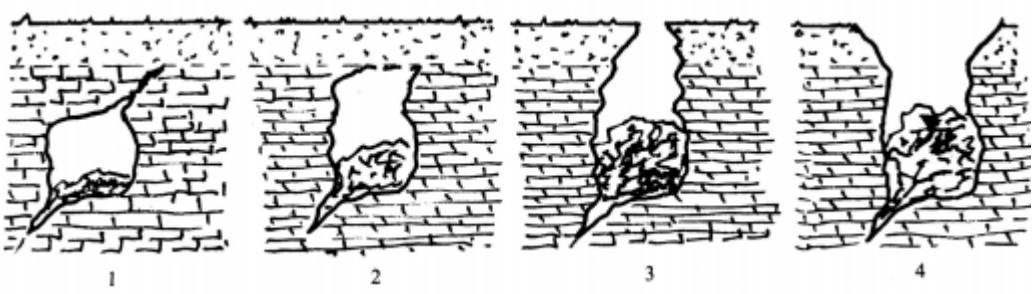


*Figure 1.1* Development of natural subsidence in limestone rock (Reddish & Whittaker, 2012)

According to Waltham (1978), the triggering mechanism for the occurrence of sinkhole was the washing down of surface sediments into underlying cavernous limestone.

North (1952) indicated that downwards flow of water in limestone makes its way through joints and bedding planes thereby giving rise to chemical weathering of rocks and widening the channels (Reddish & Whittaker, 2012).

In February 2013, a sinkhole opened up late night near Tampa Florida, swallowing a man in his bedroom. Figure 1.2 shows the house, under where the subsidence occurred. And the sinkhole exposed after the house was teared down and the debris was moved away (Figure 1.3). Therefore, the concern for the threats from sinkholes was raised.

*Figure 1.2* An engineer surveys in front of the home where a sinkhole opened up in Seffner, Florida (Memmott, 2013)

*Figure 1.3* An aerial view of the sinkhole which was exposed after the house was demolished, Seffner, Florida (Morel, 2013)

## 1.2 Research objectives and scope of work

Numerous underground cavities exist, posing unknown risks of potential failure. These risks can become threats when structures are built above these cavities, endangering property and lives.

The objective of this study is to conduct a general conceptual analysis for evaluating the stability of potentially existing underground cavities and their impact on the ground surface. This will be achieved using the modeling tools Examine 2D and Phase2 (RS2) by considering various geological properties for both cohesive soil and limestone, geometric characteristics for the void underneath the ground surface and water conditions. The study aims to generate some insightful knowledge for estimating potential failures of the ground above potential cavities under various scenarios.

The study aims at finding the minimum stable overburden thickness with a strength factor greater than 1. The unstable zone around the void is delineated by a strength factor less than 1. Figure 1.4 illustrates the research flow chart. The detailed research work includes:

- Identify the problem: The threat of underground cavities to the stability of ground surface, furthermore, to the safety of infrastructures and human lives.
- Define the objective: To study the impact of underground cavity to the ground stability by finding the minimum stable overburden thickness with strength factor greater than 1, as well as the affected area around the void with strength factor less than 1 under various scenarios and conditions.
- Make assumptions to the properties of materials: Cohesive soil and limestone, which are with different consistencies defined by cohesion and friction angle and rock qualities defined by Geological Strength Index (GSI) values, respectively.
- Water conditions: Dry and Fully saturation, as two extreme conditions.
- Two modeling scenarios of void: Fixed bottom with various heights and Fixed dimension at various elevations.
- Run the models under the above categories and analyze the results to find a general trend.
- Make conclusions and recommendations indicating the limits and possible errors, and suggestions about the future works.

It is important to note that this research is not based on any real cases.

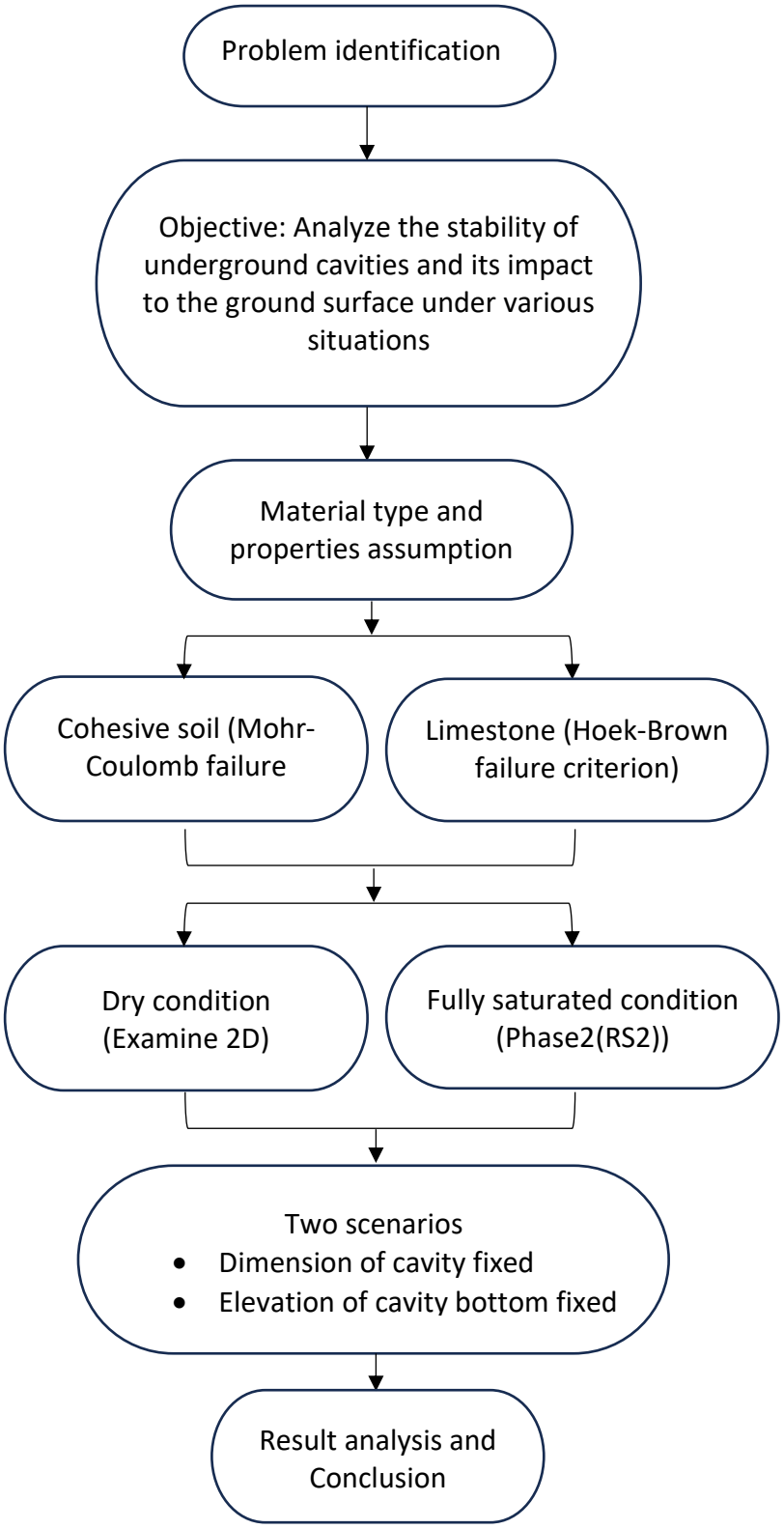


*Figure 1.4* Thesis outline

# Chapter 2 Literature Review

This chapter provides a review of the failure mechanisms of ground subsidence associated with underground openings, as well as findings from previous numerical analyses on the stability of underground cavities and ground surface.

## 2.1 Mechanism of subsidence

Prior to the surface subsidence, underground collapse or abstraction would proceed in advance. During the process, natural voids, the form of mining, degree and extent of activity coupled with geological factors will all play a role in the formation of subsidence. The creation of an underground excavation or cavity results in a re-distribution of the stress field and this reacts with the rocks or soil surrounding the excavation or cavity thereby inducing movements with collapse potential or subsequent closure which is related to time.

### 2.1.1 Ground movement associated with mine roadway or tunnel

The example shown in Figure 2.1 is a rectangular opening in a stratified geological setting, corresponding to a coal seam development drivage in a predominantly vertical stress field. Stress arch over a mine roadway in a mainly vertical stress field is formed and beds (spanning the opening) tend to sag and separate. The strata within the stress arch may collapse into voids, especially where weak mudstone beds form the immediate roof. However, if the immediate roof is strong enough, it can give longtime support and in those partial extraction methods including room and pillar mining where the pillars are stable, the risk of surface subsidence becomes small afterwards.

A stress gradient occurs between arch and dome (Figure 2.1), if it is sufficient to exceed the strength of rock in its tri-axial state of stress, fracture occurs, resulting in the stress relieved in dome which will collapse if not supported.

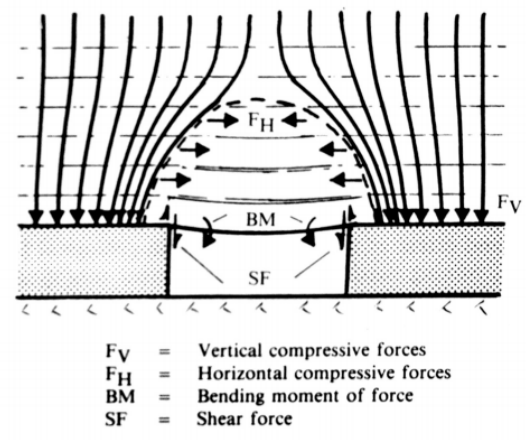


*Figure 2.1* Distribution of forces in the vicinity of the roof of a roadway according to NCB (1950-1951)

There are two common forms of ground movement associated with roadways according to Reddish and Whittaker (2012).

1) The removal of the support leads to caving of the roof strata, and the bulking of fractured rocks attempts to fill or partially fill the void.

Roof beds are subjected to various combinations of tensile, shear and compressive stress. These stresses interact with the inherent weakness within the rock structure, like slip planes, jointing, bedding planes and faulting. However, the existence of strong beds can discourage the upward collapse.

Bulking factor refers to the ratio of the volume of excavated material to the volume of the material in its in-situ (natural) state. Stronger rocks have a greater bulking factor than

weaker ones. Weaker rocks are likely to break during excavation and so produce a greater variation in particle size distribution, causing a lower buckling factor. Figure 2.2 shows the roof collapse with bulking factor 20% and 50%. 50% of bulking factor is quite common, while 20% is rarely encountered. The widths of the domes do not appear to increase significantly, as the increase in height, due to the limitation from the roadway. The occurrence of subsidence at the surface above dome in a mine roadway depends on the depth of the mine roadway. If the expansion of failed material cannot fill the cavity before reaching the surface, the ground surface will subside. In other words, if the opening is deep enough, failure of the cavity will not get to the surface due to bulking characteristics of the material.

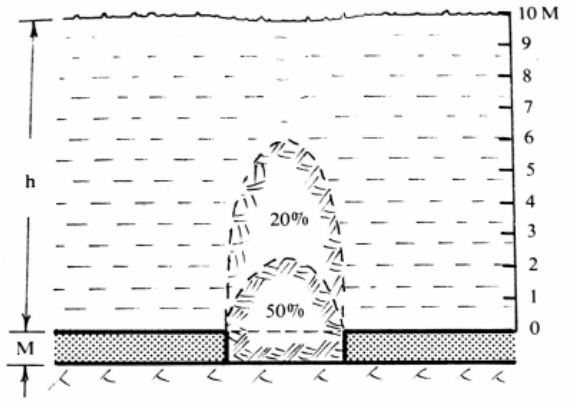


*Figure 2.2* Projected extent of collapse of mine roadway roof collapse for bulking factor 20% and 50% in stratified rocks which readily cave (Reddish & Whittaker, 2012)

2) Ground movement of unconsolidated overburden above a shallow mine roadway

Figure 2.3 illustrates that the roof collapse with unconsolidated overburden (especially sand) involves shearing above the roadway sides and a relatively confined column of material slumping downwards.

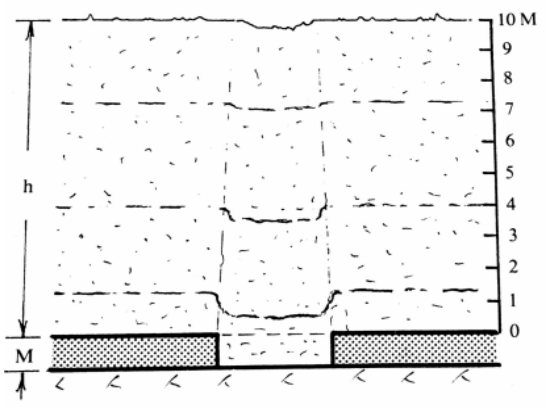


*Figure 2.3* Collapse characteristics of unconsolidated overburden (sands) into a mine roadway at a small depth (Reddish & Whittaker, 2012)

### 2.1.2 Ground movement associated with longwall extraction

The ground movement directions associated with a wide extraction such as a longwall face have been described by Grond (1951, 1957) who summarized the ideas of German and Dutch investigators up to the time of his publications. Figures 2.4 and Figure 2.5 illustrate the main points discussed by Grond (1951, 1957) concerning projected ground movements for both the transverse and longitudinal directions of a longwall. Figure 2.4 demonstrates Dutch concepts of ground movement, with general movements attracted directly towards the mined-out area with a certain amount of upward movement indicated beneath the mining horizon. Figure 2.5 is based on early German concepts of ground movement interacting with a pressure arch, or dome of relaxed ground above the extracted region. The idea is conveyed here that a break-line projected ahead of the face line turns sharply towards the face after having intercepted the pressure arch.

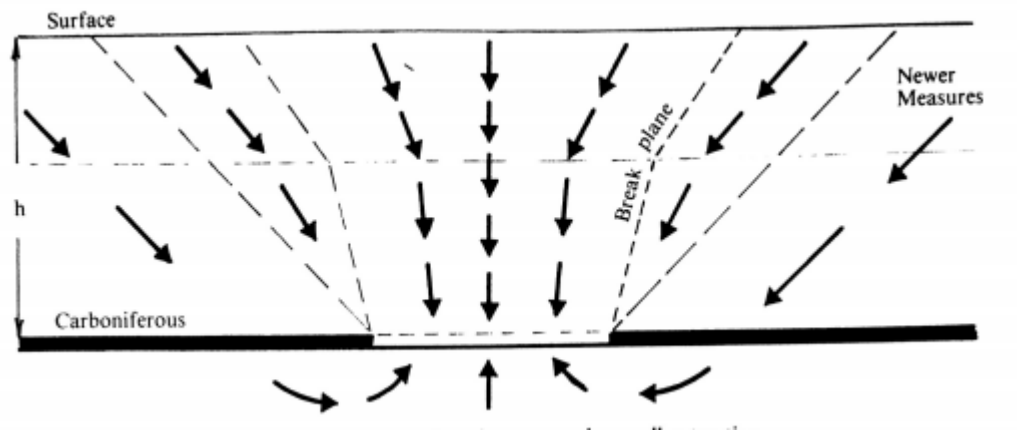


*Figure 2.4* Ground movement around a longwall extraction based on Dutch theory according to Grond (1951, 1957)

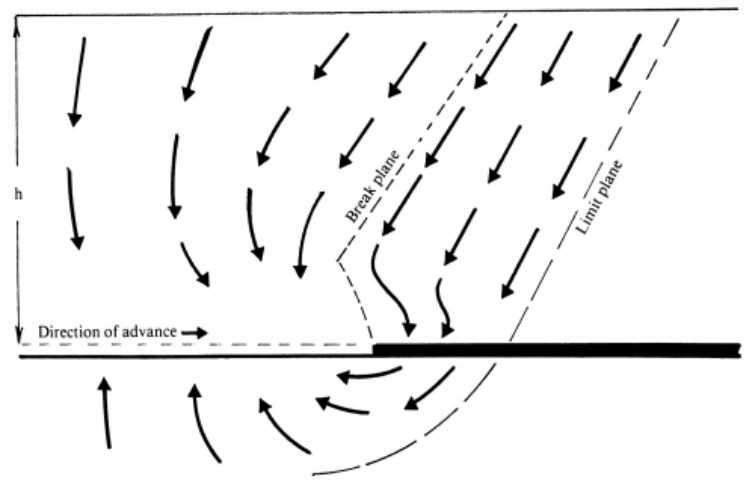


*Figure 2.5* Ground movement around advancing longwall face based on German theory according to Grond (1951, 1957)

The ground movement pattern associated with a longwall extraction based on investigations by Whittaker, Reddish and Fitzpatrick (1985) is shown in Figures 2.6 and Figure 2.7. A principal feature is the line of shearing which hades over the extracted region, and this shear line extends approximately linearly as the thickness of extraction increases. They show a tendency for ground movements to rotate around the coalface in the case of the advancing face line and this is accompanied by successive occurrence of shear line

which play a role in the mode of ground movement behind the face. The transverse section of the longwall, Figure 2.6, shows the establishment of symmetrical shear lines heading over the extraction with a rotational tendency for ground movement to occur from the rib sides. In the case of shear lines shown in Figure 2.7, these relate to the process of advancing the longwall and tend to close again at some distance behind the face line, this appears to take effect at about 1/4 to 1/3 of the depth from the surface.

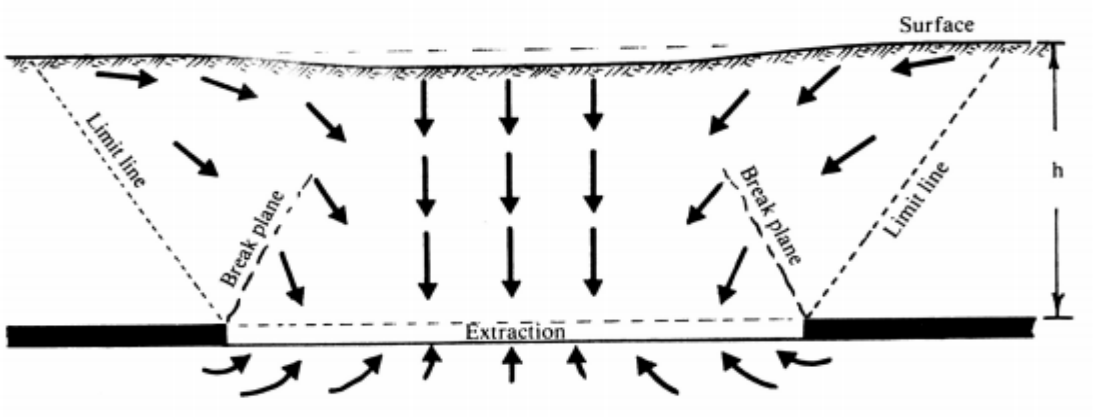


*Figure 2.6* Ground movement around a longwall extraction based on investigations from UK according to Whittaker, Reddish and Fitzpatrick (1985)

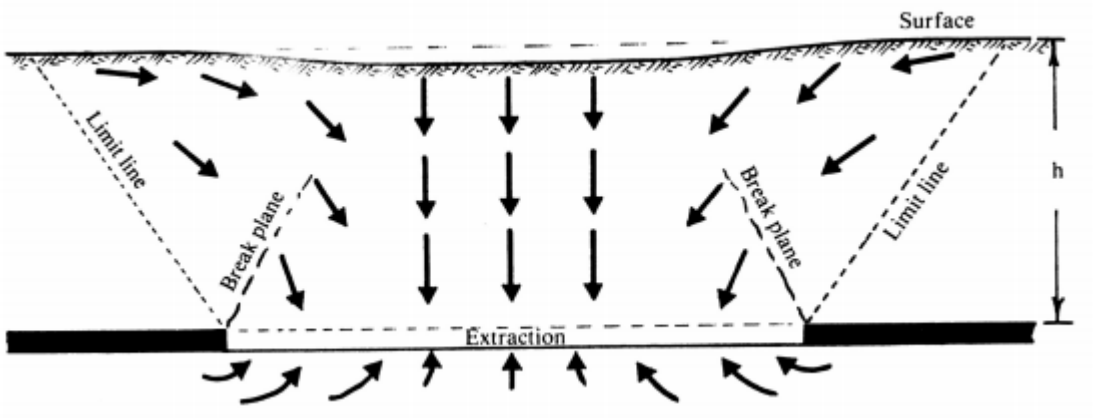


*Figure 2.7* Ground movement around advancing longwall face based on investigations from UK according to Whittaker, Reddish and Fitzpatrick (1985)

The ground movement process is related to the redistribution of strata pressure around the longwall. Figure 2.8 and Figure 2.9 show the pressure arch condition in relation to subcritical (w/h < 1.2-1.4) and supercritical (w/h >1.2-1.4) ratio extraction width (w) compared to depth (h). Figure 2.8 indicates natural arching across the extraction is taking place thus preventing full return to cover load pressure within the goaf area and such process discourages full development of surface subsidence. On the contrast, Figure 2.9 shows the pressure arch to intercept the surface, which allows fill return to cover load pressure over part of the extracted area and relates to development of maximum surface subsidence.

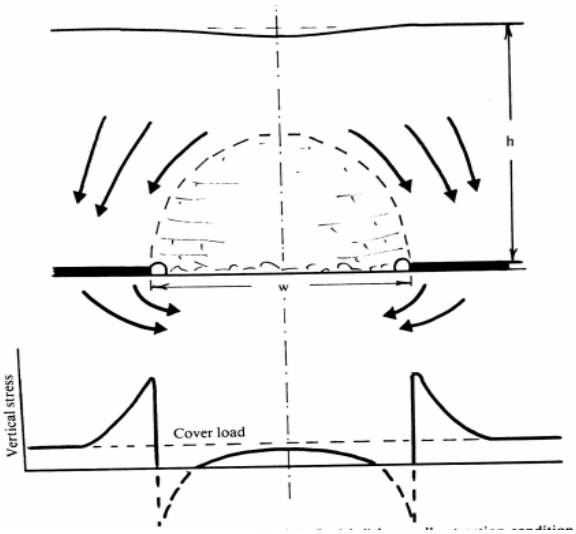


*Figure 2.8* Pressure arch in relation to sub-critical (w/h < 1.4) longwall extraction condition (Whittaker & Pye, 1977)

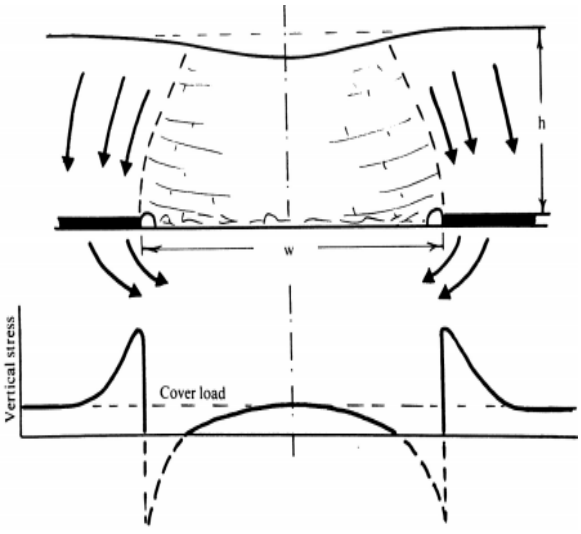


*Figure 2.9* Pressure arch in relation to super-critical (w/h > 1.4) longwall extraction condition (Whittaker & Pye, 1977)

## 2.2 Numerical modeling attempts in stability analysis of underground cavities and sinkhole formation

Numerical studies were carried out by researchers to simulate the subsidence phenomena and analyze the stability of underground voids and ground surface. They have provided insights into the factors that influence failure behavior, such as geological conditions, void dimensions, and material properties.

Augarde et al. (2003) predicted the collapse of a submerged undrained spherical cavity which resulted in the characteristic surface depression often referred to as a sinkhole. They were focusing on the effects of the depth (C) over the diameter (D) of the void as shown in Figure 2.10.

Conventional dimensional analysis of the six basic problem variables $\{\sigma_T, \sigma_S, C, D, \gamma, c_u\}$ yields four dimensionless groups (Butterfield, 1999).

$$\left\{\frac{\sigma_T}{c_U}, \frac{\sigma_S}{c_u}, \frac{C}{D}, \frac{\gamma D}{c_u}\right\} \qquad \text{Equation 1}$$

where,

$\sigma_T$ = Internal pressure

$\sigma_S$ = Vertical surcharge

$C$ = Depth of the cavity (measured from the ground surface to the top of the cavity)

$D$ = Diameter of the cavity

$\gamma$ = Unit weight

$c_u$ = Undrained shear strength

As mentioned by Augarde et al. (2003), the first two groups can be combined into the single group $(\sigma_S - \sigma_T)/c_u$ which is so-called the load parameter, as they are dependent due to the assumption of undrained behaviour. They found that stability was affected only by the difference between $\sigma_S$ and $\sigma_T$.

Finite-element limit analysis has been employed to give rigorous bounds on a suitable load parameter $(\sigma_S - \sigma_T)/c_u$ with which it is possible to assess the stability of a cavity under undrained conditions. And they have created charts used to obtain upper and lower bound values of the load parameter $(\sigma_S - \sigma_T)/c_u$ given values of the weight parameter $(\gamma D)/c_u$ and geometry parameter C/D.

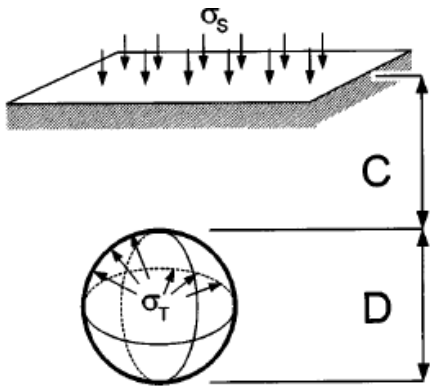


*Figure 2.10* Layout of sinkhole formation problem by Augarde et al. (2003)

Depth/width ratio (h/w) is one of the factors to be considered during the calculation of factor of safety (Lamb & Shiau, 2014; Mirza, 2019) for a rectangle shape underground cavity, where h is the overburden thickness and w represents the width of cavity (Figure 2.11).

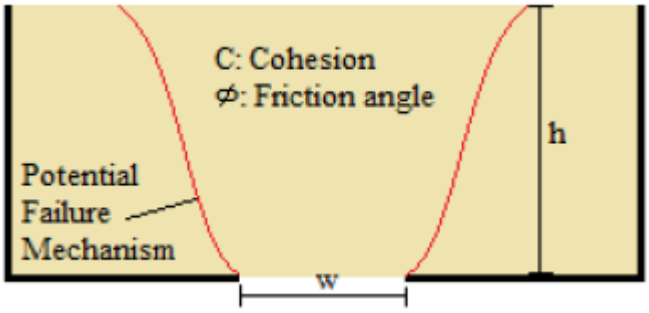


*Figure 2.11* Idealized sinkhole formation in 2D view. (Lamb & Shiau, 2014)

Lamb et al. (2014) studied the effects from the saturation level, they concluded that drained sand had an immediate failure no matter how the depth/width ratio changed due to cohesionless property. The undrained clay and cohesive soil showed an increase trend of factor of safety as the depth/width ratio went up (Figure 2.12 and Figure 2.13). The cohesive soil demonstrated the highest stability among all the scenarios.

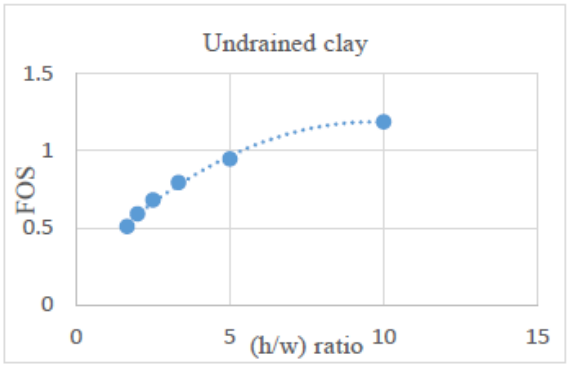


*Figure 2.12* Factor of safety vs depth/width ratio (h/w) plot for undrained clay (Lamb et al., 2014)

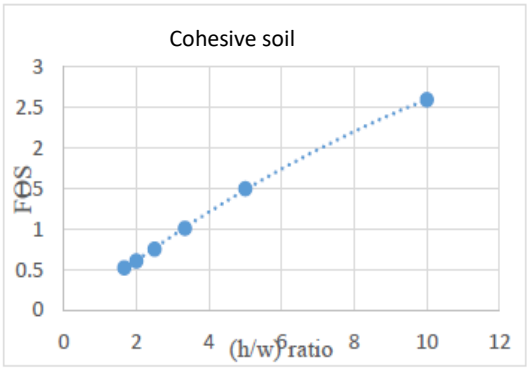


*Figure 2.13* Factor of safety vs depth/width ratio (h/w) plot for cohesive soil (Lamb et al., 2014)

Mirza (2019) generated a trend line to determine the failure extent with the depth/width ratio for undrained clay, which is shown in Figure 2.14, where E is the failure extent

exposed on the ground surface, H is the depth of the underground opening and W is the width of the opening.

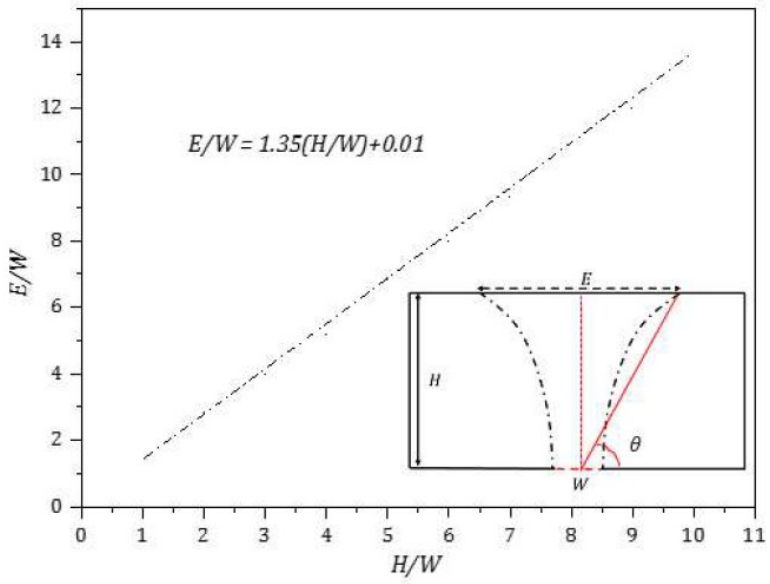


*Figure 2.14* Design chart for the determination of failure extent (Mirza, 2019)

He also studied the relationship between factor of safety (FoS) for the upper boundary of the opening and the depth/width ratio (H/W). As shown in Figure 2.15, he found that the FoS value decreases nonlinearly as the depth/width ratio (H/W) increases. Indeed, for the homogeneous cohesive soil with a constant shear strength ratio $S_u/(\gamma W)$, the increase of overburden pressure (γH) would reduce the stability, and thus the value of FoS. $S_u$ is the undrained shear strength and $\gamma$ is unit weight of the material in his study. This suggests that none or very little arching support is developed for the current study of homogeneous cohesive soils with zero internal soil frictional angle (ψ).

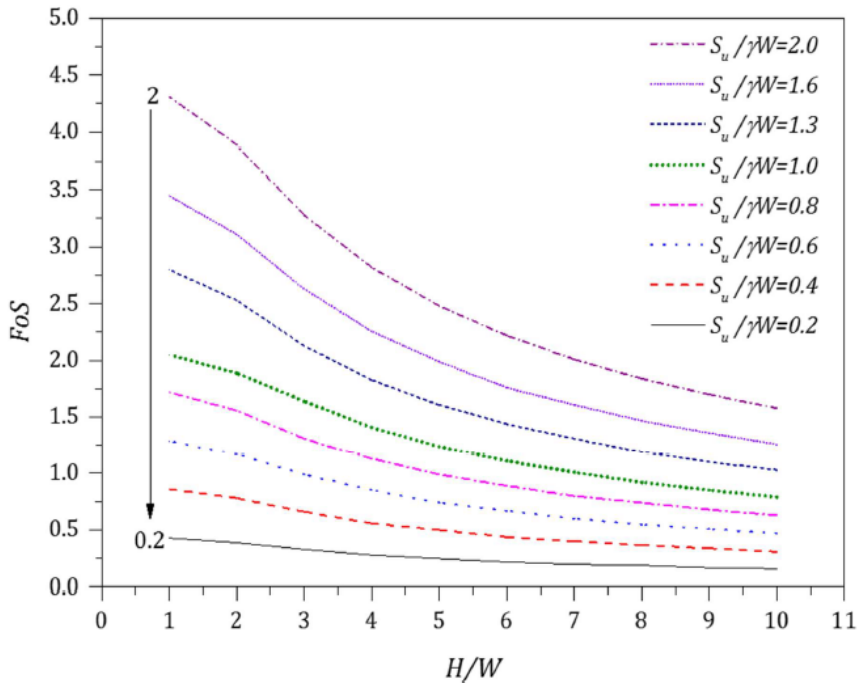


*Figure 2.15* Factor of safety vs depth/width ratio (H/W) (Mirza, 2019)

Another research focused on the influence of the change of distance between the underground cavity located in cohesive soil and the ground surface, the change in height and width of the cavity to the total displacement of the ground surface with or without foundation on the ground. (Taleb & Guemidi, 2023). It came out the total displacement is almost proportional to the increase in width and increases linearly with the increase in height.

Similarly, by defining the stability of materials with strength factor (S.F.) (equivalent to the factor of safety) in modeling, my research aims to analyze stability of the overburden based not only on the location but also the dimension of the void. Additionally, the study considers various conditions such as materiel types (cohesive soil and limestone), different consistencies and qualities of materials surrounding the cavity and water conditions. The difference compared with what has been done by other researchers is

that instead of observing the strength factor itself, the contour lines generated by strength factor which encloses the unstable zone around the void and the stable zone in the overburden are what have been analyzed in this study.

# Chapter 3 Research Methodology

This chapter introduces the analysis methods utilized in the research and modeling procedures, also gives explanation on preparation of the models, selection of material types & properties, investigated scenarios, and definition of failure zone & relevant indicators for stability evaluation.

## 3.1 Analysis method

The research was conducted using a comprehensive numerical modeling process, incorporating two Rocscience software tools to analyze and simulate the behavior of underground cavity considering different material properties and water conditions. One of the software tools is Examine 2D, utilizing the boundary element analysis method, while the other is Phase2, which is based on finite element method.

### 3.1.1 Boundary element method (BEM)

The BEM is a numerical computational method of solving linear partial differential equations which have been formulated as integral equations (i.e. in boundary integral form).

The attraction of the BEM is generally attributed to the reduction in the dimensionality of the problem. For two-dimensional problems, only the line boundary of the domain needs to be discretized into elements (Aliabadi, 2020), in terms of which, the computational time of the modeling and solution processing is much less in comparison to the finite element method and other domain-type technique (Aliabadi, 2020; Mirza, 2019).

### 3.1.2 Finite element method (FEM)

The FEM is a general numerical method for solving partial differential equations in two or three space variables (i.e., some boundary value problems). To solve a problem, the FEM subdivides a large system into smaller, simpler parts called finite elements. This is achieved by a particular space discretization in the space dimensions, which is implemented by the construction of a mesh of the object: the numerical domain for the solution, which has a finite number of points. The finite element method formulation of a boundary value problem finally results in a system of algebraic equations. The method approximates the unknown function over the domain. The simple equations that model these finite elements are then assembled into a larger system of equations that models the entire problem. The FEM then approximates a solution by minimizing an associated error function via the calculus of variations.

## 3.2 Model preparation

### 3.2.1 Material properties assumption

The research considered two materials under both dry and fully saturated conditions: cohesive soil and limestone. For soil, models were created to analyze different levels of consistencies by varying combinations of cohesion and friction angle. As well as rock qualities with Geological Strength Index (GSI) values from low to high. The detailed properties of cohesive soil and limestone are presented in Chapters 4.1 and 5.1, respectively.

### 3.2.2 Software introduction

#### *3.2.2.1 Examine 2D*

Examine2D is a 2-dimensional plane strain indirect boundary element program for the elastic stress analysis of underground excavations.

It is a parametric analysis tool for investigating the influence of geometry and in-situ stress variability on the stress changes in rock due to excavations. The induced stresses in the plane of the analysis can be viewed by means of stress contour patterns in the region surrounding the excavations. As a tool for interpreting the amount of deviatoric overstress (principal stress difference) around openings, strength factor contours give a quantitative measure of (strength)/ (induced stress) according to a user defined failure criterion for the rock mass. The analysis procedure is listed as follows:

- Project settings: Analysis type, units, project summary, etc.
- Create internal excavation boundaries
- Generate stress grid
- Assign material properties
- Define field stresses and external loads
- Interpret the results

#### *3.2.2.2 Phase 2 (RS2)*

Phase 2 is a 2-dimentional modeling analysis software based on finite element method. The analyzed area will be divided into small elements (triangle elements with six nodes in this case). Software carries out failure analysis on each node using all the parameters

provided, and the final results such as principal stresses, total displacement and strength factor will be shown as contours in the graph after computation. The analysis procedure is listed as follows:

- Project settings: Analysis type, units, stages, etc.
- Create the boundaries: Internal and external boundary
- Apply boundary conditions
- Define field stresses
- Assign materiel properties
- Run the model and interpret the results

#### *3.2.2.3 Software selection*

Compared to RS2, Examine2D generates the results faster due to BEM, so it was used to work through models built up for single material in dry conditions. However, in terms of the limit that Exmaine2D can only be used for dry conditions, RS2 models have been created for fully saturated water conditions.

### 3.2.3 Model design and development.

The cavity was designed to be horseshoe-shape shown in Figure 3.1, which can be simulated as an underground tunnel, natural cavity or mine working. The width of the void in the model was set to be 9 m. The height of the wall was 5.5 m. And the roof is arc-shape with radius of 4.5 m. Two conners of the bottom were cut out at the shape of isosceles triangle, the legs' length of which was 0.5 m, to avoid influence from stress

concentration. The size and shape of the cavity may not be the same as a particular cavity but provide a base for general analysis.

Furthermore, on top of the ground, there assumes to be a 12 m × 12 m two-storey house with weight of approximately 72300 kg, so the corresponding pressure is 4 kN/m$^2$. The location of house could be anywhere. In this study, a typical but not specific location where the wall of the building aligns with the center of the cavity was chosen, which is easier to locate the cavity from the building. In 2D view, the vertical stress coming from the building is distributed for 12 m, the boundary of which aligns with the center line of the void.

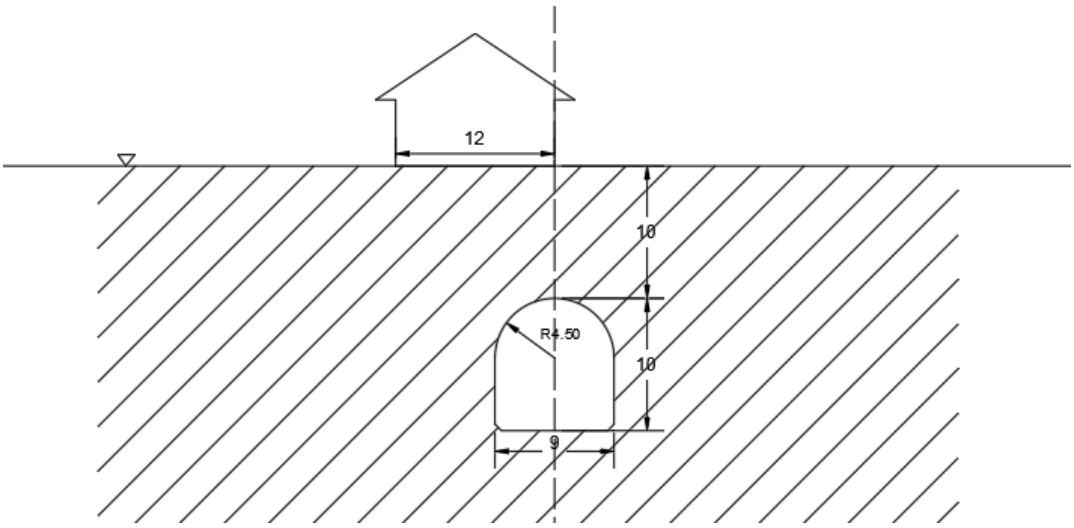


*Figure 3.1* Vertical cross-section 2D sketch of the model showing a house located above an underground cavity

#### *3.2.3.1 Examine 2D model*

Although the external boundary of stress grid will not have influence on the stress distribution around the boundary of the cavity, the stress grid is still set to be large enough (120 m in width and 100 m in depth) to cover all the models to be analyzed in program.

Examine 2D performs the boundary element method analysis immediately upon the creation of the exaction model. The results are interpreted directly after inputting all relevant parameters. In Figure 3.2, a representative interpretation of strength factor contours is presented.

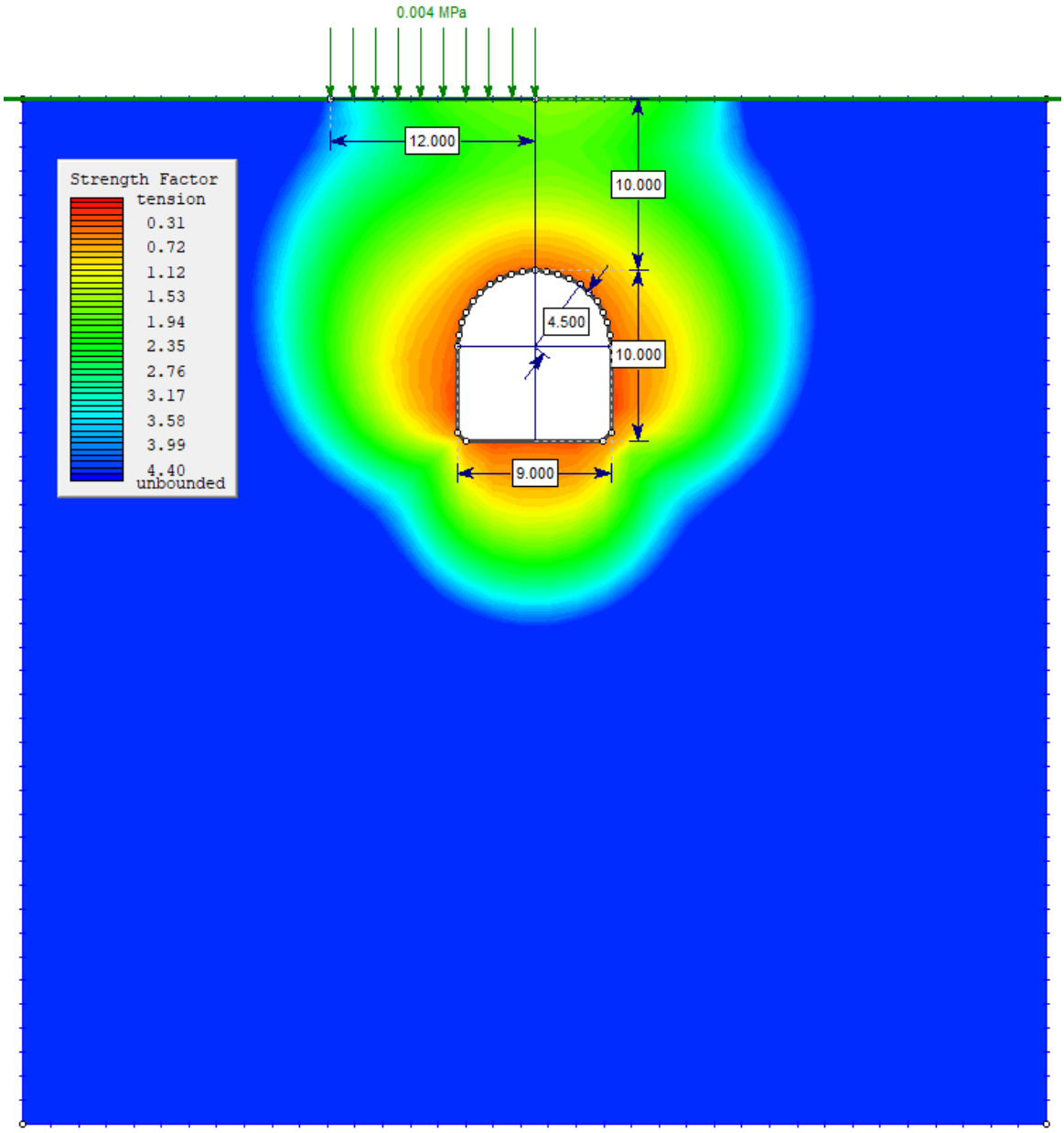


*Figure 3.2* Sample output contours of strength factor generated by Examine2D

### *3.2.3.2 Phase 2 model*

Phase 2 (RS2) is based on FEM, which means unlike Examine 2D, the boundary of the model has influence on the stress distribution around the void. Therefore, to avoid the influence caused by external boundary, the width and height of the external boundary have to be at least five times greater than dimensions of internal boundary of the void. In this study, the underground cavity was 9 m in width, and the bottom of which may go down to 50 m underneath ground surface. After comparing results from different external dimensions and results generated by Examine 2D, the width of external boundary was set to be 240 m and the height was 300 m (Figure 3.3). Default number of nodes on the external boundary was set to be 540. 6 node-triangle of element type was applied in the model.

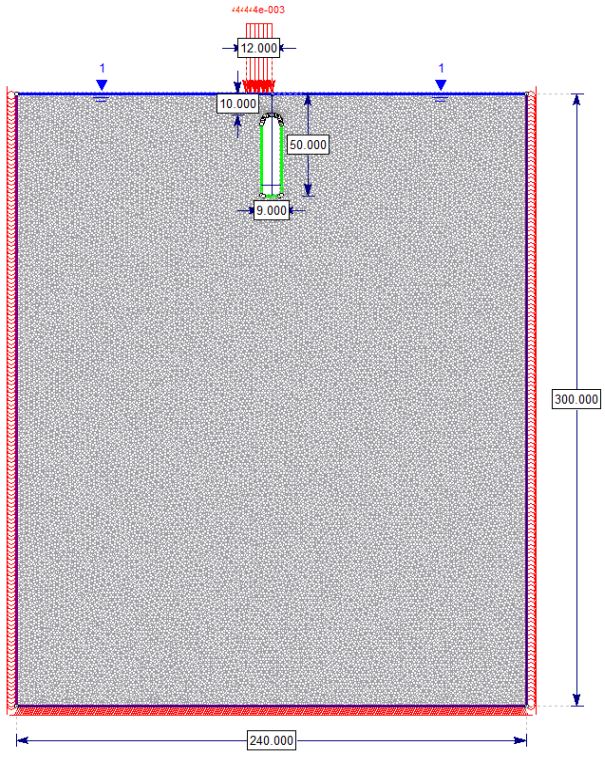


*Figure 3.3* Sample model created by RS2

Since RS2 models were for fully saturated water conditions, water table was applied to the ground surface. The HU coefficient is simply a factor between 0 and 1, by which the vertical distance from a point (in the soil or rock) to a water surface (i.e. Piezo Lines) is multiplied to obtain the pressure head. The HU value is used to calculate pore pressure as follows:

$$u = \gamma_w h HU \qquad \text{Equation 2}$$

where,

$u$ = Pore pressure

$\gamma_w$ = The pore fluid unit weight (entered in the Project Settings dialog)

$h$ = The vertical distance from a point to a piezometric line

$HU$ = The HU value for the material

When HU equals to 0, it indicates a dry soil or limestone. HU = 1 would indicate hydrostatic conditions, which means the soil or limestone is 100% saturated with water.

There are restrictions for the external boundary conditions in order to simulate the real situation. Both sides of the boundary are restrained in horizontal direction and the bottom is both horizontally and vertically restrained, so that the deformation of ground can only be able to move upwards or inwards the cavity.

Being different from Examine 2D, RS2 needs to run the computation and interpretation to get the results shown in a newly generated separate window. Figure 3.4 shows the strength factor contour output for the model shown in Figure 3.3.

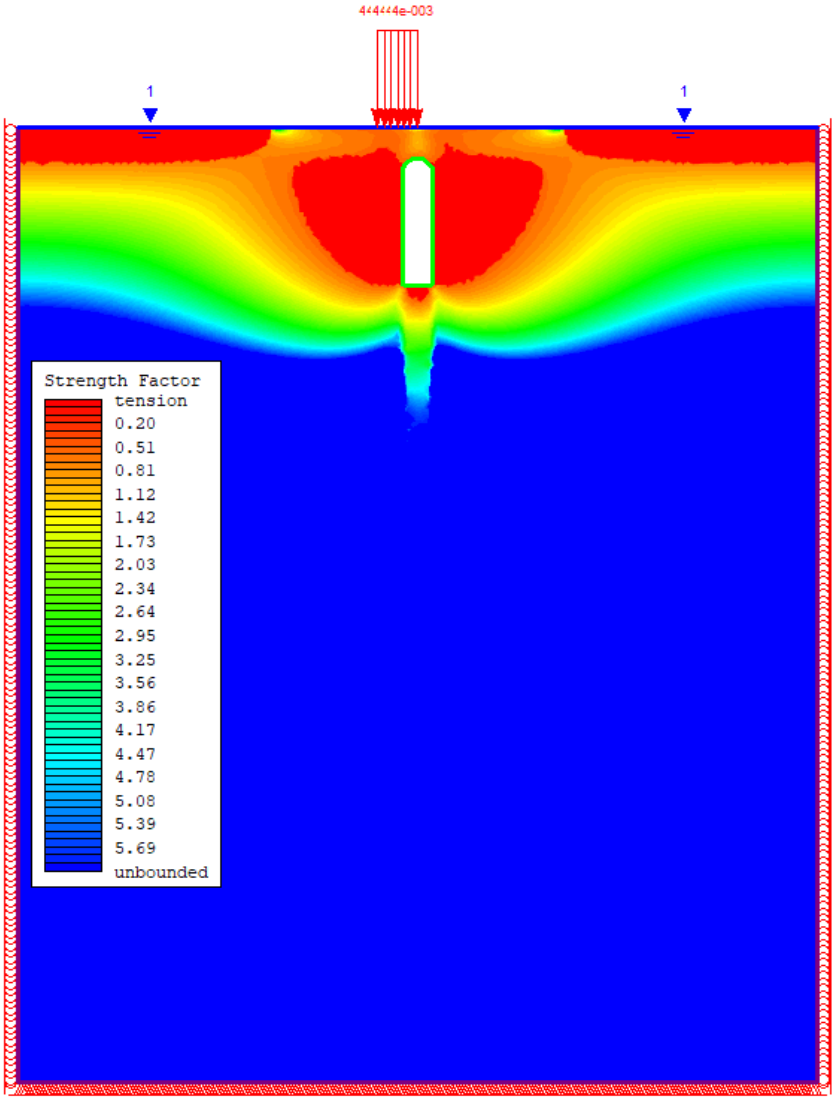


*Figure 3.4* Sample output contours of strength factor generated by RS2

### 3.2.4 Definition of failure zone and relevant indicators

The strength factor (S.F.) is generally used to evaluate the stability of ground and rock mass, which is defined as

$$S.F = \frac{Material\ strength}{Induced\ stress}$$ Equation 3

The overburden may collapse into the cavity when S. F≤1. Therefore, critical points separating S.F. ≤ 1 from S.F. > 1 have been located to determine the boundary of potential failure area.

In this research, two indicators have been analyzed to determine the stability of above and around the void, which are $H_1$ (Safe zone depth) and $H_2$ (Maximum weak zone height) (Figure 3.5). H is the thickness of overburden. The existence of safe zone within overburden directly reflects the stability of the ground, while weak zone height exhibits the scale of unstable area around the void, giving an insight of potential failure and sinkhole growth. Also, these indicators can be the reference for reinforcement.

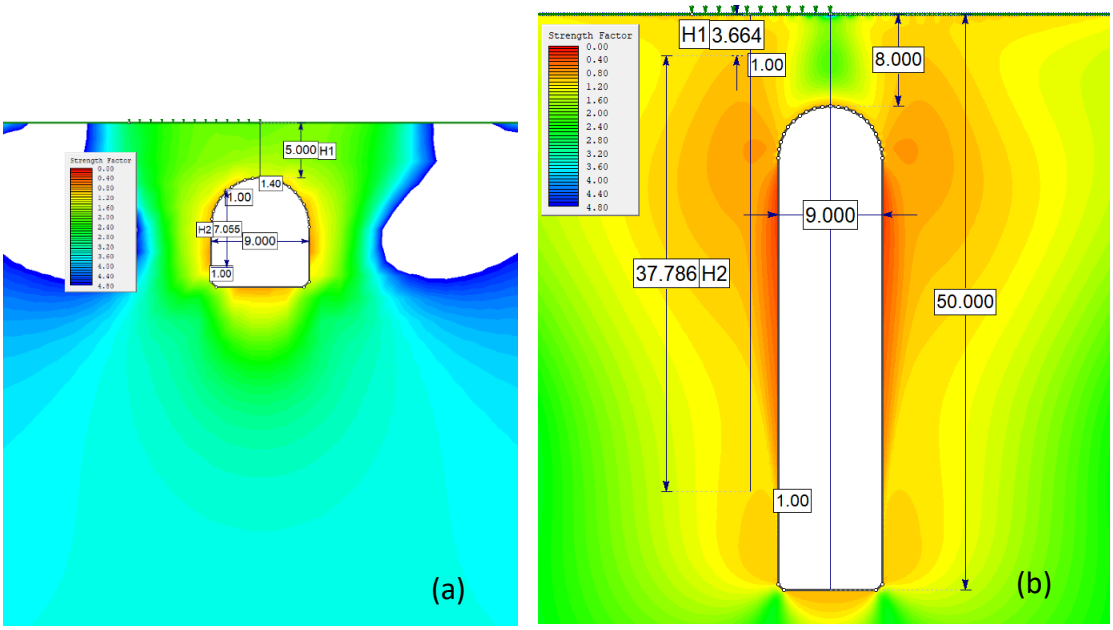


*Figure 3.5* Two Sample models generated with Examine 2D illustrating the definition of each indicator: (a) Fixed dimension ;(b) Fixed bottom

Figure 3.5(a) and Figure 3.5(b) present the model and simulation results under 'Fixed

bottom' and ‘Fixed bottom’ scenarios, respectively.

They are demonstrated as examples at same scale to give explanations on all the data being analyzed. Figure 3.5(a) shows a 9 meter-wide and 10 meter-high cavity located 5 m under the ground surface in limestone. The material assigned in Figure 3.5(b) is the same as in Figure 3.5(a). The differences are dimensions and elevations of the cavity. It is 9 m in width and 42 m in height and the overburden thickness is 8 m in Figure 3.5(b).

$H_1$ represents the depth measured from the ground surface to the location where the S.F. grows to the point exactly bigger than 1, and that location must be above the cavity, either to the sides of it or right on the roof.

$H_2$ is measured from the top of the contour with S.F. ≥ 1 to the bottom point of the same contour alongside the walls of the cavity.

## 3.3 Modeling scenarios

There are two scenarios considered in general while building the models. For both scenarios, all the combinations of properties under different soil consistencies and rock qualities were analyzed.

1) The first one, ‘Fixed bottom’ scenario, involves changing elevation of the roof while keeping bottom of the cavity at a specific level (50 m below ground surface in this research). It tends to simulate voids with different heights or the growth of a collapsed void with the roof fallings into the cavity. Figure 3.6 shows three sample types of the model to be analyzed.

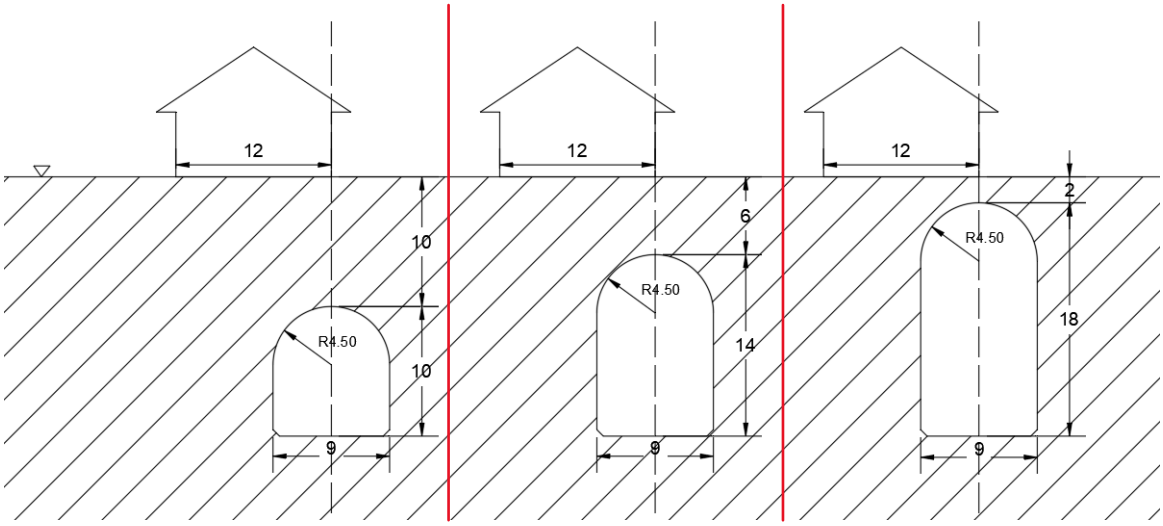


*Figure 3.6* First scenario with bottom fixed at -50 m

2) The second scenario, 'Fixed dimension', is to alter the vertical location of the void when keeping the dimension constant (Height= 10 m, width= 9 m). Three sample types with the same void size but at different elevations are shown in Figure 3.7. This scenario is to provide insight into the voids that may be located at various depths underneath the infrastructure.

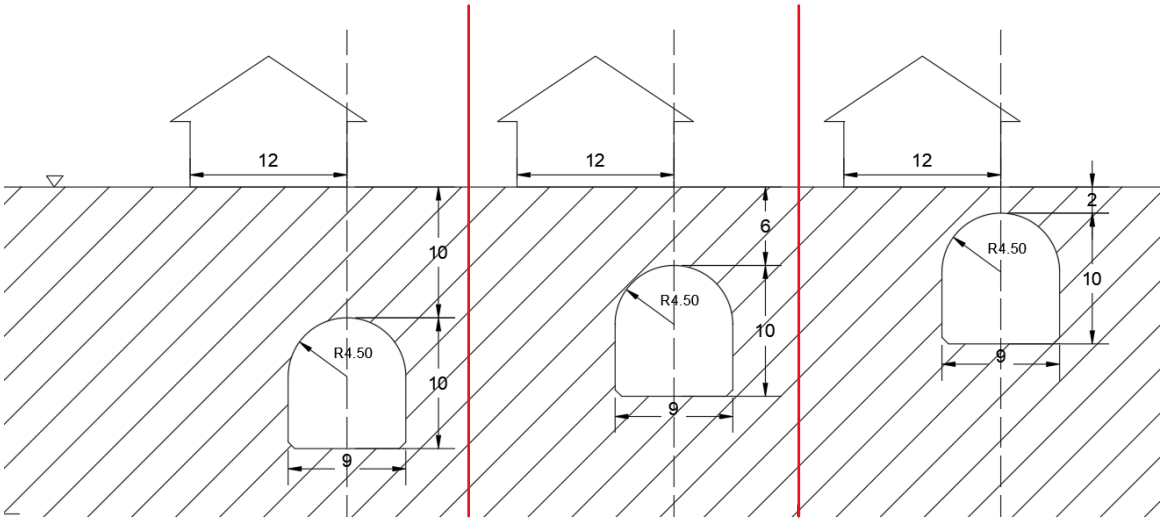


*Figure 3.7* Second scenario with dimension fixed at $H_o$=10 m, $W_o$=9 m

# Chapter 4 Numerical Simulation and Stability Analysis of Underground Cavity in Cohesive Soil

This chapter delves into the numerical simulation and stability analysis in cohesive soil. By simulating different scenarios, including 'Fixed bottom' and 'Fixed dimension' scenarios, different water conditions and soil consistencies defined by cohesion and friction, this chapter aims to provide a comprehensive assessment of the ground surface stability associated with underground cavities in cohesive soil.

## 4.1 Soil properties used in modeling

To simulate realistic scenarios, cohesionless soil such as sandy soil was not considered in this research. The study focused on three different types of cohesive soil (silt, clay, etc.) from soft to dense. And the soil material modeled was assumed to be homogenous and linearly elastic. The Mohr-Coulomb failure criterion was applied to the soil materials used in numerical modeling.

The main considerations to define consistency of soil in study were cohesion and friction angle while other input parameters were set to be average value to simplify the model. Gravitational field stress was applied to the model, and the ratio ($K_o$) of horizontal to vertical effective stresses (known as the Coefficient of Earth Pressure at Rest) was 1 (Rocscience, n.d.). According to Bowles (1997), the average unit weight was set to be 18 $kN/m^3$. The average Poisson's ratio was 0.45 (Bowles, 1997). The average Young's modulus was 20000 kPa (COE. 1990). From de Sousa Oliveira et al (2020) and Fang and Hirst (1973), the approximately average tensile strength assigned for the cohesive soil was

10 kPa. The average unconfined compressive strength for soft, medium and dense soil were 36 kPa, 70 kPa and 144 kPa, respectively (Terzaghi et al., 1996). There are correlations for unconfined compressive strength with shear strength as estimated from the filed using Vane Shear Tests which is shown in equation 4. (Knappett & Craig, 2019)

$$c = {}^{q_u}/_{2} \qquad \text{Equation 4}$$

where,

$c$ = Cohesion, kPa

$q_u$ = Unconfined compressive strength, kPa

Hence, the values of cohesion were 18 kPa, 35 kPa and 72 kPa. Friction angles varied from 17° to 28° (Ortiz et al., 1986). In general, there is a negative correlation between cohesion and friction angle , which means materials with low friction angles tend to have high cohesion, and vice versa (Knappett & Craig, 2019). Therefore, the assigned parameters of soil properties are listed in Table 4.1 after converting units as software requires.

*Table 4.1* Soil properties used in numerical modeling

| Material | consistency | Unit Weight (MN/m³) | Young's Modulus (MPa) | Tensile Strength (MPa) | Poisson's Ratio | Cohesion (kPa) | Friction Angle (°) |
|---|---|---|---|---|---|---|---|
| Soil | Soft | 0.018 | 20 | 0.01 | 0.45 | 18 | 28 |
| | Medium | | | | | 35 | 24 |
| | Dense | | | | | 72 | 17 |

## 4.2 Stability analysis under dry condition

### 4.2.1 Fixed bottom

When bottom of the void was fixed at 50 m depth underground, the elevation of roof was altered to locate the point where the safe zone appears in overburden. During which, $H_1$ and $H_2$ were determined accordingly and the trend of relationship between H and each indicator was analyzed.

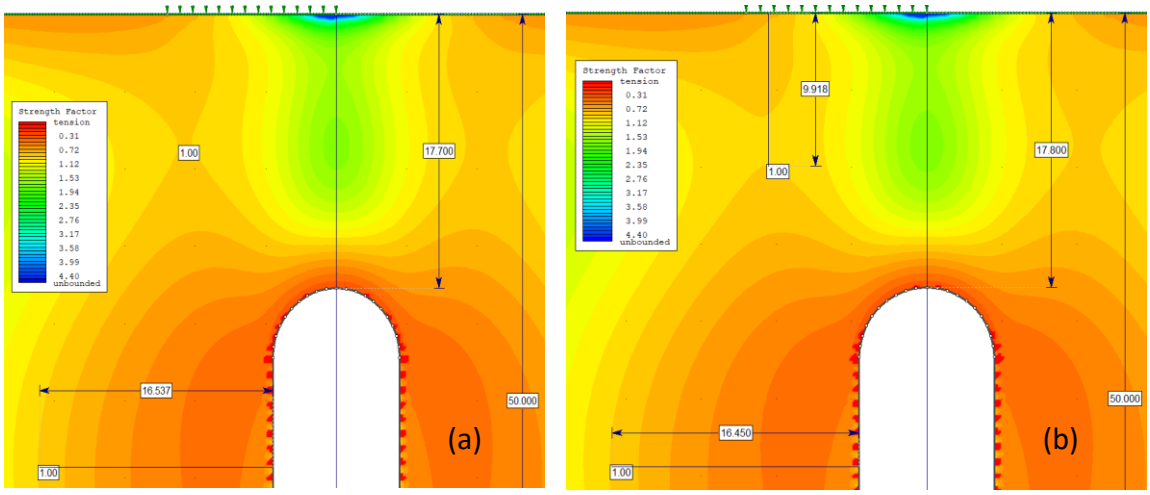


*Figure 4.1* Emerging of safe zone above the cavity when thickness of overburden ≥ 17.8 m: (a)H=17.7 m; (b)H=17.8 m

Figure 4.1 shows an example of the case where cohesion equals to 35 kPa and friction angle is 24°. In this sample model, the width of the void is 9 m, and the height changes from 32.3 m to 32.2 m. As is shown from contours in Figure 4.1, safe zone appears while H is changed from 17.7 m to 17.8 m. Consequently, $H_1$ changes from 0 m to 9.91 m. $H_2$ appears. H varies from 15 m to 40 m, and the data observed for $H_1$ are listed in Table 4.2. Thirty-five models were built in total.

Four sample models in Figure 4.2 show the changes of S.F. contour when H equals to 15 m, 17 m, 20 m and 30 m, respectively. No values of maximum weak zone height ($H_2$) were observed for all soil models, which is because $H_2$ is always bigger than the void height (H). When $H_2$ was investigated, the focus was on the extensive portion around the void that was potentially unstable. If the whole area surrounding the void is potentially unstable, then a comprehensive reinforcement strategy might be required for the entire cavity.

*Table 4.2* Observed $H_1$ when c=35 kPa, ψ=24° for dry cohesive soil under fixed bottom scenario

| H (m) | 15 | 16 | 17 | 17.5 | 17.6 | 17.7 | 17.8 | 17.9 | 18 | 19 | 20 | 30 | 40 |
|---|---|---|---|---|---|---|---|---|---|---|---|---|---|
| $H_1$ (m) | 0 | 0 | 0 | 0 | 0 | 0 | 9.91 | 10.69 | 11.34 | 14.46 | 16.34 | 27.4 | 37.45 |

Note: H—Overburden thickness; $H_1$—Safe zone depth.

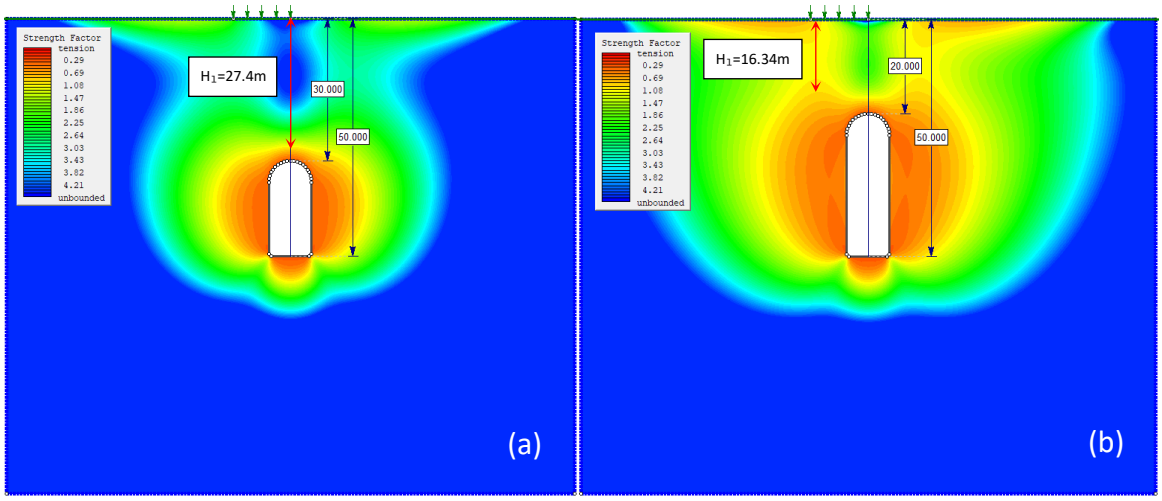

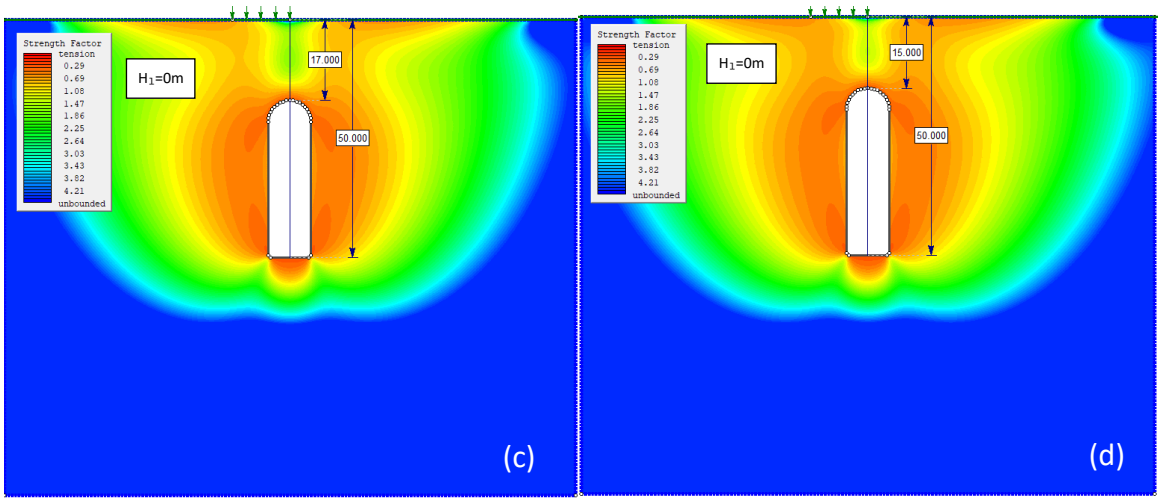


*Figure 4.2* S.F. contour of sample models with fixed bottom in dry cohesive soil when c=35 kPa, ψ=24 °: (a)H=30 m; (b)H=20 m; (c)H=17 m; (d)H=15 m

Using the same way, data were observed for soft soil with cohesion 18 kPa and friction equates 28° and dense soil with cohesion 72 kPa and friction angle 17° (Table 4.3 and Table 4.4). Safe zones show up when H is 17.7 m and 15.9 m, respectively.

*Table 4.3* Observed $H_1$ when c=18 kPa, ψ=28° for dry cohesive soil under fixed bottom scenario

| H(m) | 15 | 17 | 17.5 | 17.6 | 17.7 | 17.8 | 17.9 | 18 | 20 | 30 | 40 |
|---|---|---|---|---|---|---|---|---|---|---|---|
| $H_1$(m) | 0 | 0 | 0 | 0 | 10.40 | 11.44 | 12.01 | 12.45 | 17.08 | 27.83 | 37.79 |

Note: H—overburden thickness; $H_1$—Safe zone depth.

*Table 4.4* Observed $H_1$ when c=72 kPa, ψ=17° for dry cohesive soil under fixed bottom scenario

| H(m) | 15 | 15.5 | 15.6 | 15.7 | 15.8 | 15.9 | 16 | 17 | 20 | 30 | 40 |
|---|---|---|---|---|---|---|---|---|---|---|---|
| $H_1$(m) | 0 | 0 | 0 | 0 | 0 | 4.37 | 4.75 | 8.41 | 15.59 | 26.88 | 36.88 |

Note: H—Overburden thickness; $H_1$—Safe zone depth.

Figure 4.3 shows the relationship between $H_1$ and H. Safe zone shows up after overburden thickness is over a specific value. When H is greater than 18 m, the safe zone depth increases rapidly as the overburden thickness increases. The trendlines for dry cohesive

soil with three different consistencies converge then become parallel to each other and present linear relationships.

According to the results shown in Figure 4.3, when overburden thickness is less than 18 m, the increase of the cohesion will increase the stiffness of soil, which leads to the decrease of overburden thickness to achieve the formation of safe zone. When above 18 m, the increase of material stiffness would reduce the safe zone depth, though there is no significant difference. A possible explanation is as going deeper, friction factor plays more important role in determining the safe zone depth $H_1$. So after comparing all the trendlines and data, the thickness of overburden has to be over 17.7 m considering the lowest consistency of soil to secure the sabilization of ground surface in the first place.

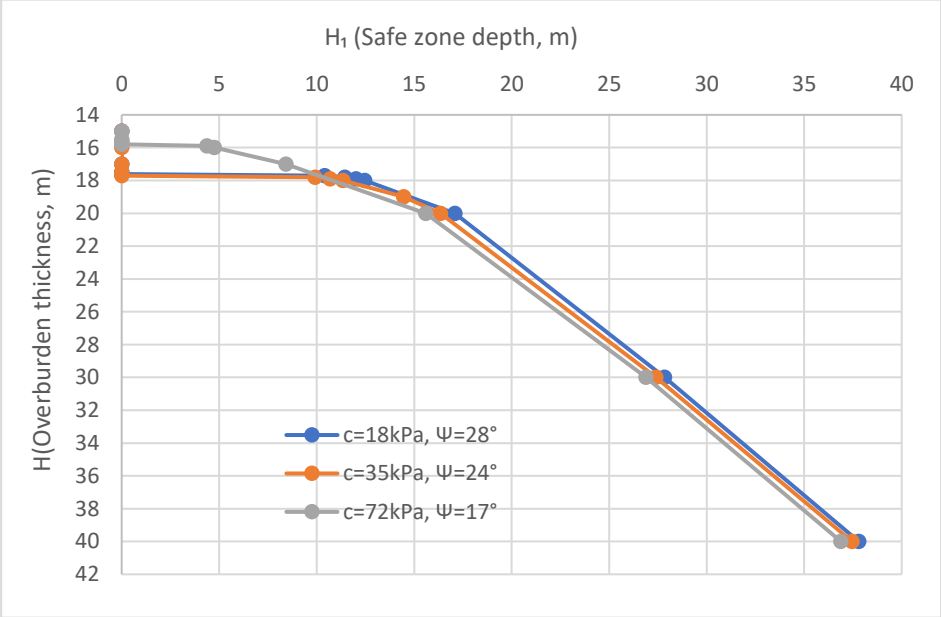


*Figure 4.3* Relationship between $H_1$ and H for dry cohesive soil with different consistency under fixed bottom scenario

### 4.2.2 Fixed dimension

In this scenario, dimension of the void is fixed at height ($H_o$) 10 m and width ($W_o$) 9 m. By modifying vertical location of the void, groups of $H_1$ and $H_2$ are identified. The range of overburden thickness H was set from 1 m to 15 m, and results collected from modeling for different consistencies are listed in Table 4.5, Table 4.6 and Table 4.7, respectively.

*Table 4.5* Observed $H_1$ when c=35 kPa, ψ=32° for dry cohesive soil under fixed dimension scenario

| H(m) | 1 | 2 | 3 | 4 | 5 | 6 | 7 | 10 | 15 |
|---|---|---|---|---|---|---|---|---|---|
| $H_1$(m) | 0 | 0 | 1.07 | 1.94 | 3.03 | 4.07 | 5.02 | 7.94 | 12.80 |

Note: H—Overburden thickness; $H_1$—Safe zone depth.

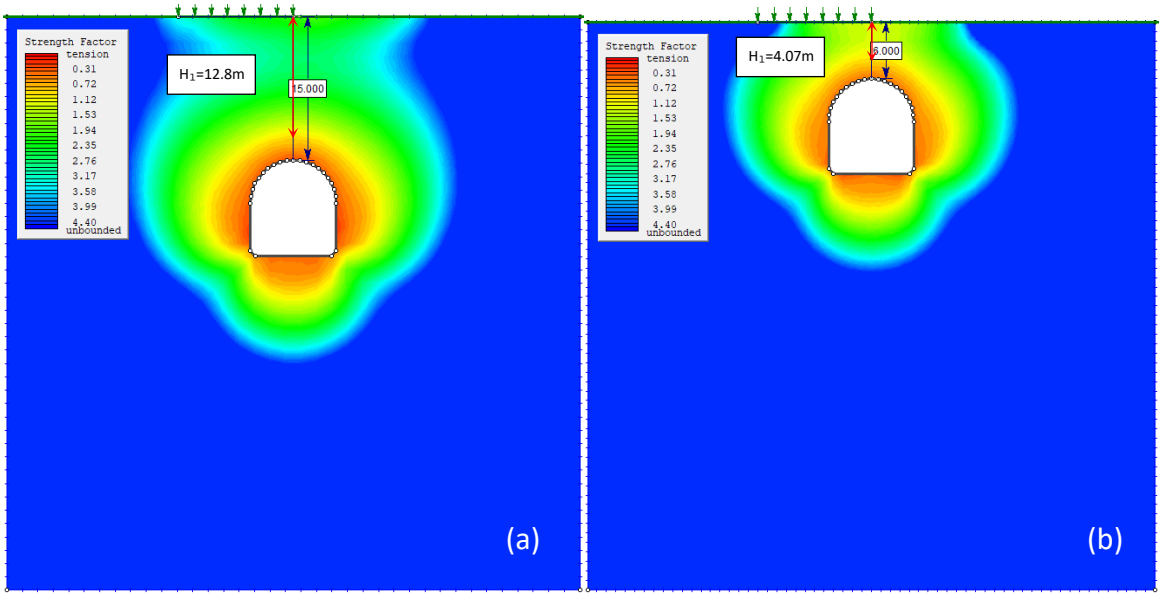

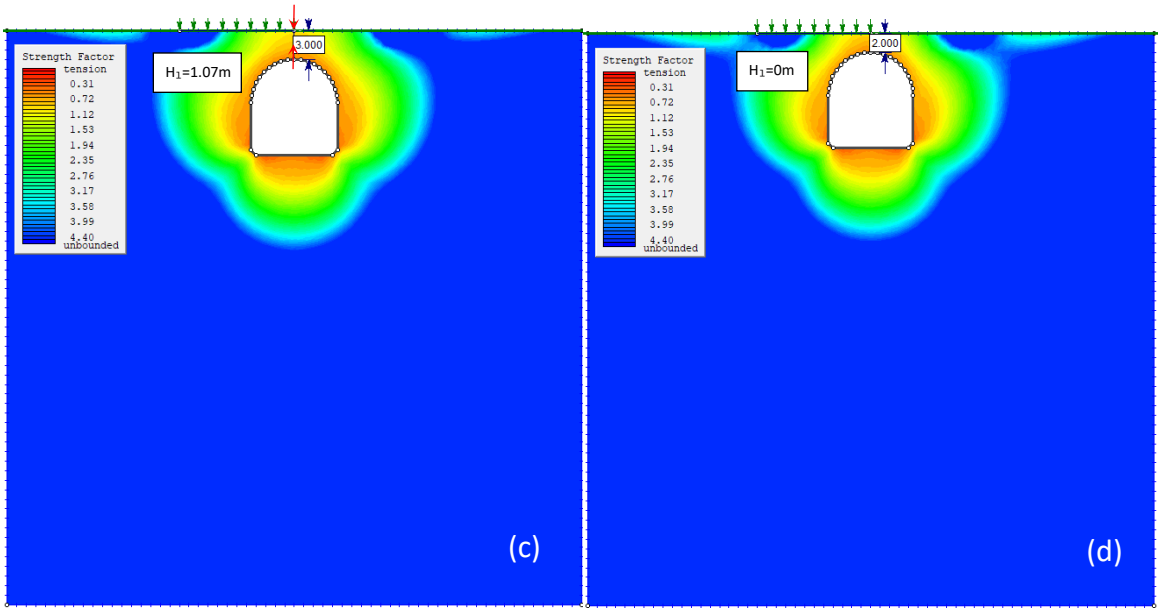


*Figure 4.4* S.F. contour of sample models with fixed dimension in dry cohesive soil when c=35 kPa, ψ=24 °: (a)H=15 m; (b)H=6 m; (c)H=3 m; (d)H=2 m

Twenty-seven models were built in total. Figure 4.4 shows the distribution of S.F. contour around four sample voids with same dimension ($H_o$=10 m, $W_o$=9 m), but different elevations which are H=2 m, 3 m, 6 m and 15m respectively.

*Table 4.6* Observed $H_1$ when c=18 kPa, ψ=28° for dry cohesive soil under fixed dimension scenario

| H(m) | 1 | 2 | 3 | 4 | 5 | 6 | 7 | 10 | 15 |
|---|---|---|---|---|---|---|---|---|---|
| $H_1$(m) | 0 | 0 | 0 | 0.15 | 1.28 | 3.50 | 4.49 | 7.81 | 12.83 |

Note: H—Overburden thickness; $H_1$—Safe zone depth.

*Table 4.7* Observed $H_1$ when c=72 kPa, ψ=17° for dry cohesive soil under fixed dimension scenario

| H(m) | 1 | 2 | 3 | 4 | 5 | 6 | 7 | 10 | 15 |
|---|---|---|---|---|---|---|---|---|---|
| $H_1$(m) | 0 | 1.57 | 2.16 | 3.21 | 4.02 | 4.93 | 5.719 | 8.39 | 12.93 |

Note: H—Overburden thickness; $H_1$—Safe zone depth.

Figure 4.5 suggests that for dense soil (c=72 kPa), safe zone appears when overburden thickness is larger than 2 m. And for soft soil, safe zone shows up when overburden

thickness is greater than 4 m, which means to ensure the stability of ground surface, the thickness of overburden must be at least 4 m.

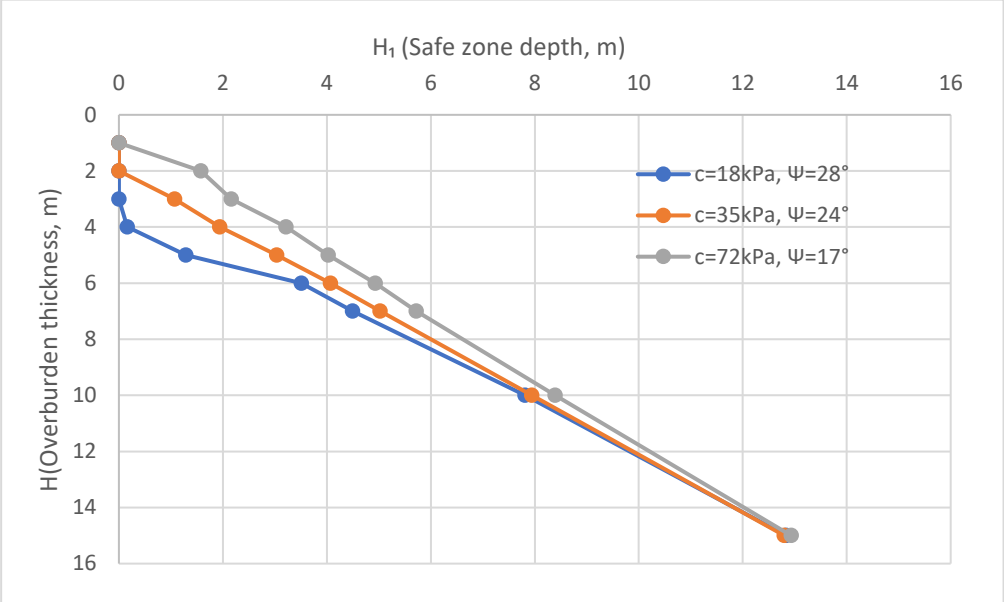


*Figure 4.5* Relationship between $H_1$ and H for dry cohesive soil with different consistency under fixed dimension scenario

## 4.3 Stability analysis under fully saturated condition

### 4.3.1 Fixed bottom

Thirty models were built in total. Figure 4.6 shows four samples of strength factor contours when H equals to 40 m, 30 m, 19 m and 16 m, respectively, in which situations cohesion is 35 kPa, friction angle is 24 ° and the bottom is fixed at 50 m depth. Different from dry models, water table and 100% saturated water condition were applied.

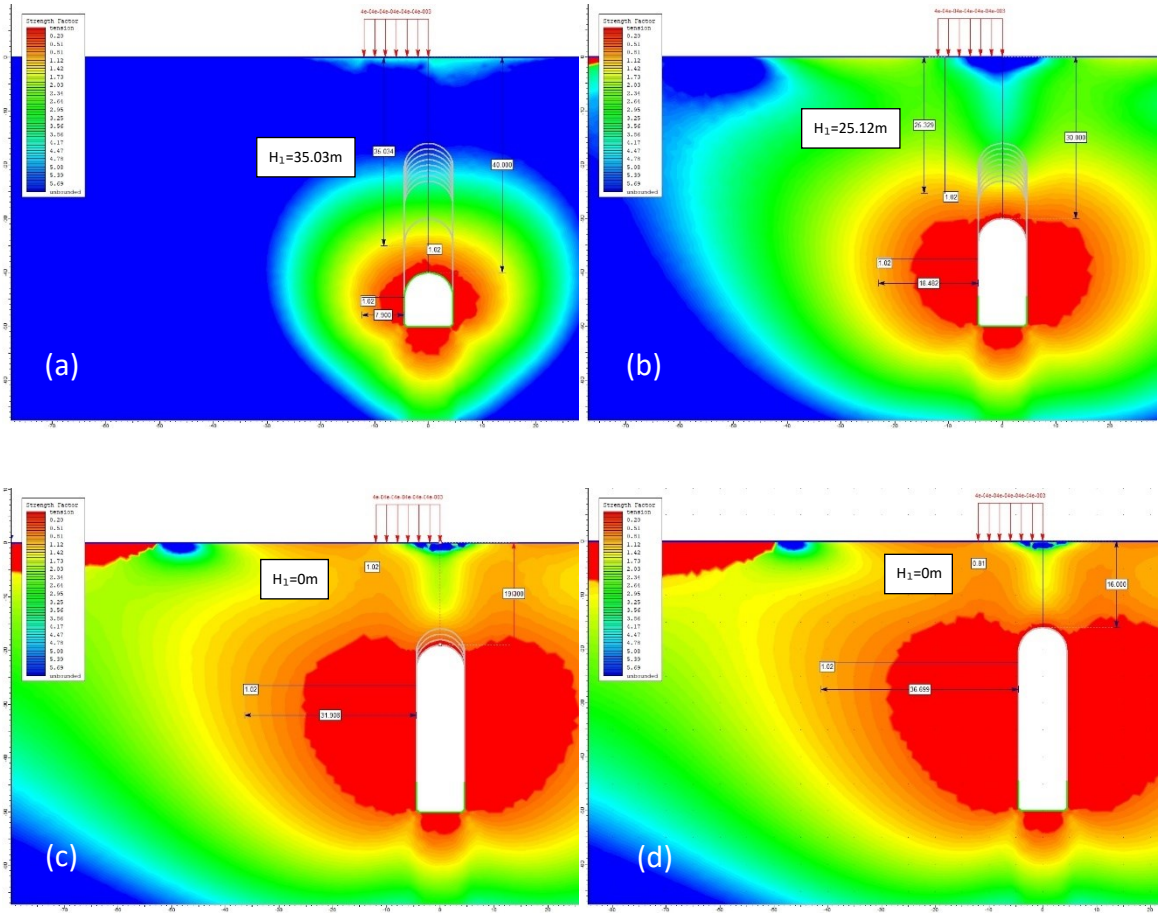


*Figure 4.6* S.F. contour of sample models with fixed bottom in fully saturated cohesive soil when c=35 kPa, ψ=24 °: (a)H=40 m; (b)H=30 m; (c)H=19 m; (d)H=16 m

Observed data for soft, medium and stiff cohesive soil under fully saturated condition are listed in Table 4.8, Table 4.9 and Table 4.10. Safe zones appear when H are greater than 21 m, 19 m and 14 m for soft, medium and stiff cohesive soil, respectively.

*Table 4.8* Observed $H_1$ when c=18 kPa, ψ=28° for 100% saturated cohesive soil under fixed bottom scenario

| H(m) | 20 | 21 | 22 | 23 | 24 | 25 | 26 | 30 | 35 | 40 |
|---|---|---|---|---|---|---|---|---|---|---|
| $H_1$(m) | 0 | 0 | 11.40 | 14.16 | 15.98 | 17.72 | 19.20 | 25.12 | 30.78 | 35.19 |

Note: H—Overburden thickness; $H_1$—Safe zone depth.

*Table 4.9* Observed $H_1$ when c=35 kPa, ψ=24° for 100% saturated cohesive soil under fixed bottom scenario

| H(m) | 16 | 17 | 18 | 19 | 20 | 21 | 22 | 23 | 30 | 40 |
|---|---|---|---|---|---|---|---|---|---|---|
| $H_1$(m) | 0 | 0 | 0 | 0 | 8.03 | 11.43 | 13.65 | 15.40 | 25.32 | 35.03 |

Note: H—Overburden thickness; $H_1$—Safe zone depth.

*Table 4.10* Observed $H_1$ when c=72 kPa, ψ=17° for 100% saturated cohesive soil under fixed bottom scenario

| H(m) | 13 | 14 | 15 | 16 | 17 | 18 | 19 | 20 | 30 | 40 |
|---|---|---|---|---|---|---|---|---|---|---|
| $H_1$(m) | 0 | 0 | 0 | 5.87 | 7.83 | 9.87 | 11.50 | 12.89 | 25.84 | 34.99 |

Note: H—Overburden thickness; $H_1$—Safe zone depth.

Figure 4.7 shows the relationship between $H_1$ and H under fully saturated condition. Like dry conditions, safe zones suddenly appear, and the depth increases rapidly as the overburden thickness increases when smaller than 22 m. Then, the trendlines converge towards a single point.

The decrease in the stiffness of soil would result in increase of overburden thickness to achieve the formation of safe zone. When overburden thickness is greater than 23 m, denser the soil is, higher the safe zone depth. After comparing all the trendlines and data, the thickness of overburden has to be over 14 m considering the lowest consistency of soil to secure the sabilization of ground surface under fully saturated condition in the first place.

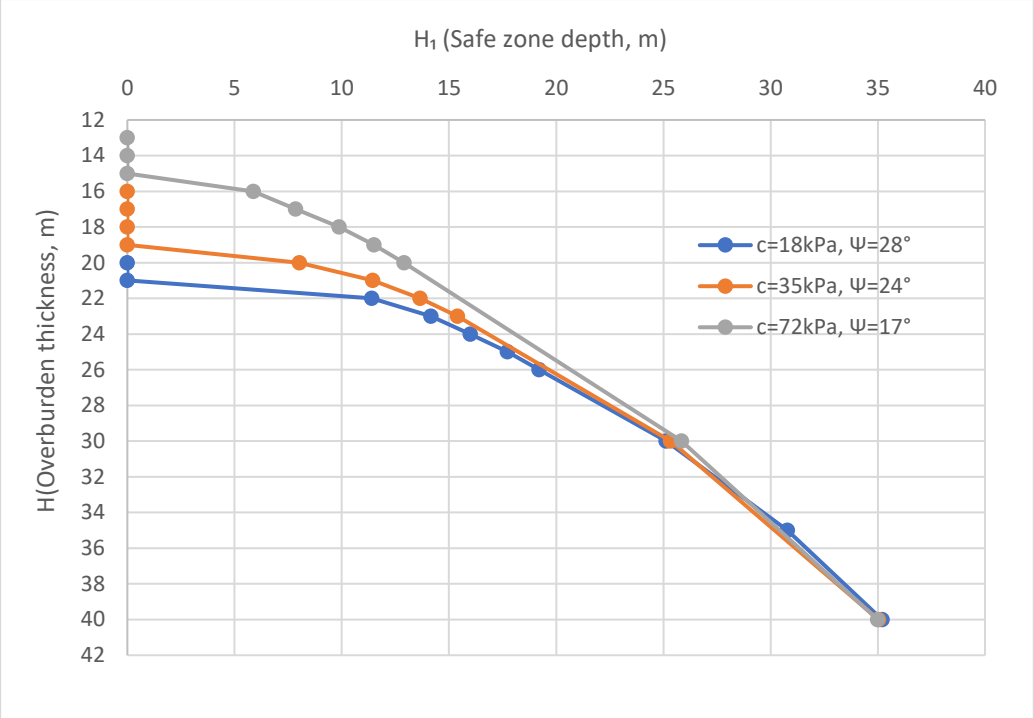


*Figure 4.7* Relationship between $H_1$ and H for 100% saturated cohesive soil with different consistency under fixed bottom scenario

### 4.3.2 Fixed dimension

Thirty-six fully saturated models were built in total. Four models are introduced as samples in Figure 4.8, of which the overburden thicknesses are 20 m, 10 m, 5m and 1 m, respectively. Same to dry condition, within fixed dimension scenario, the width of the void is kept at 9 m and height at 10 m.

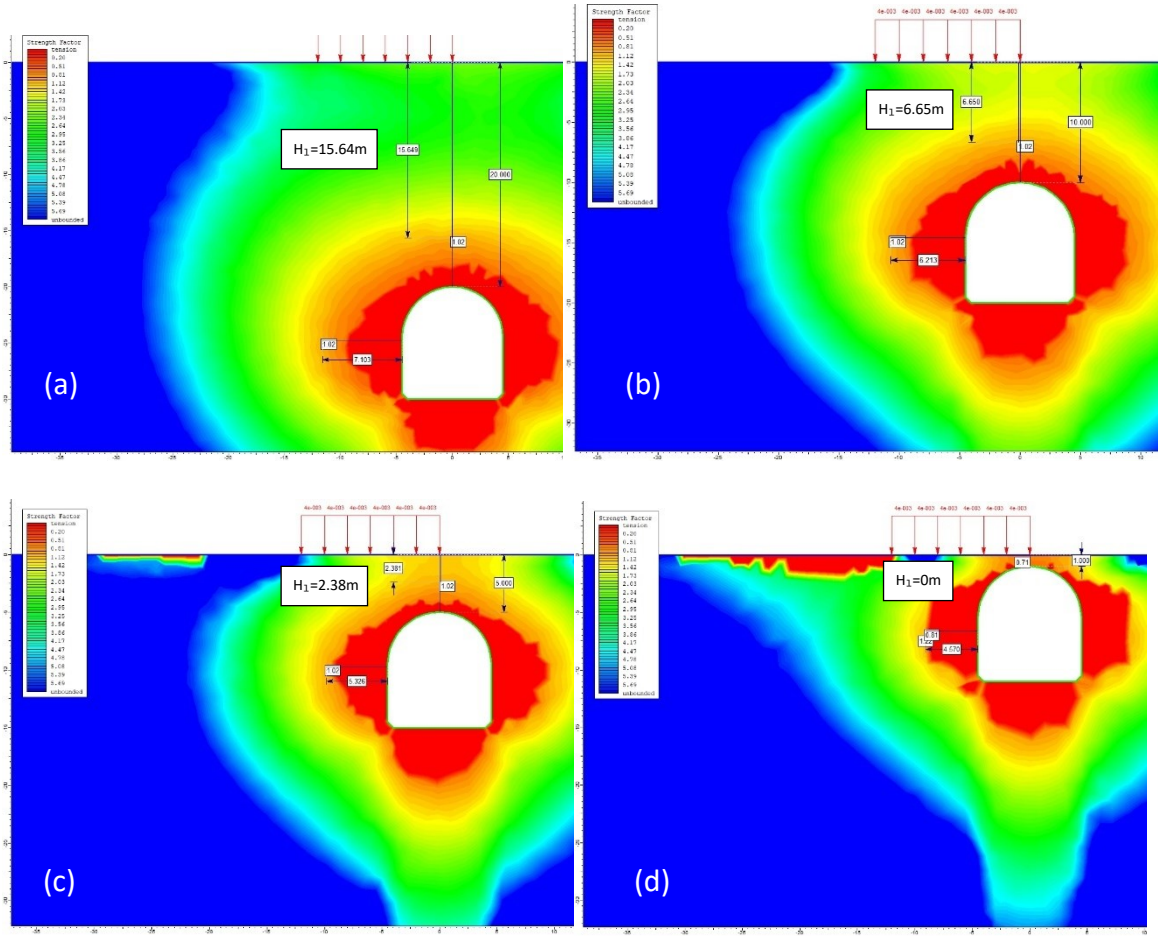


*Figure 4.8* S.F. contour of sample models with fixed dimension in fully saturated cohesive soil when c=35 kPa, ψ=24 °: (a)H=20 m; (b)H=10 m; (c)H=5 m; (d)H=1 m

The observed data for soft, medium and dense soil are recorded in Table 4.11, Table 4.12 and Table 4.13, respectively.

*Table 4.11* Observed $H_1$ when c=18 kPa, ψ=28° for 100% saturated cohesive soil under fixed dimension scenario

| H(m) | 1 | 2 | 3 | 4 | 5 | 6 | 7 | 8 | 9 | 10 | 15 | 20 |
|---|---|---|---|---|---|---|---|---|---|---|---|---|
| $H_1$(m) | 0 | 0 | 0 | 0 | 0 | 0 | 0 | 3.53 | 4.56 | 5.66 | 10.53 | 15.41 |

Note: H—Overburden thickness; $H_1$—Safe zone depth.

*Table 4.12* Observed $H_1$ when c=35 kPa, ψ=24° for 100% saturated cohesive soil under fixed dimension scenario

| H(m) | 1 | 2 | 3 | 4 | 5 | 6 | 7 | 8 | 9 | 10 | 15 | 20 |
|---|---|---|---|---|---|---|---|---|---|---|---|---|
| $H_1$(m) | 0 | 0 | 0 | 1.52 | 2.38 | 3.36 | 4.01 | 4.90 | 5.79 | 6.65 | 11.06 | 15.64 |

Note: H—Overburden thickness; $H_1$—Safe zone depth.

*Table 4.13* Observed $H_1$ when c=72 kPa, ψ=17° for 100% saturated cohesive soil under fixed dimension scenario

| H(m) | 1 | 2 | 3 | 4 | 5 | 6 | 7 | 8 | 9 | 10 | 15 | 20 |
|---|---|---|---|---|---|---|---|---|---|---|---|---|
| $H_1$(m) | 0 | 1.21 | 2.23 | 2.87 | 3.72 | 4.52 | 5.25 | 6.13 | 6.98 | 7.76 | 12.03 | 16.24 |

Note: H—Overburden thickness; $H_1$—Safe zone depth.

Same to fixed dimension scenario under dry condition, all three curves exhibit positive correlation between $H_1$ and H, which means that as the void locates deeper down underground, safe zone depth increases as well (Figure 4.9). They all experience linear relationship after certain depth, -1 m for dense soil, -4 m for medium soil and -8 m for soft soil from observation.

The biggest difference is due to the presence of water, the reduction of effective stresses and strength of the material lead to the increase of overburden thickness to ensure the appearance of safe zone above cavity, which stands for the stability of ground surface. Compared to dry model, the stable depth for soft soil increases from 4 m to 8 m. So, the thickness of overburden is required to be over 8 m to guarantee the stability of ground surface.

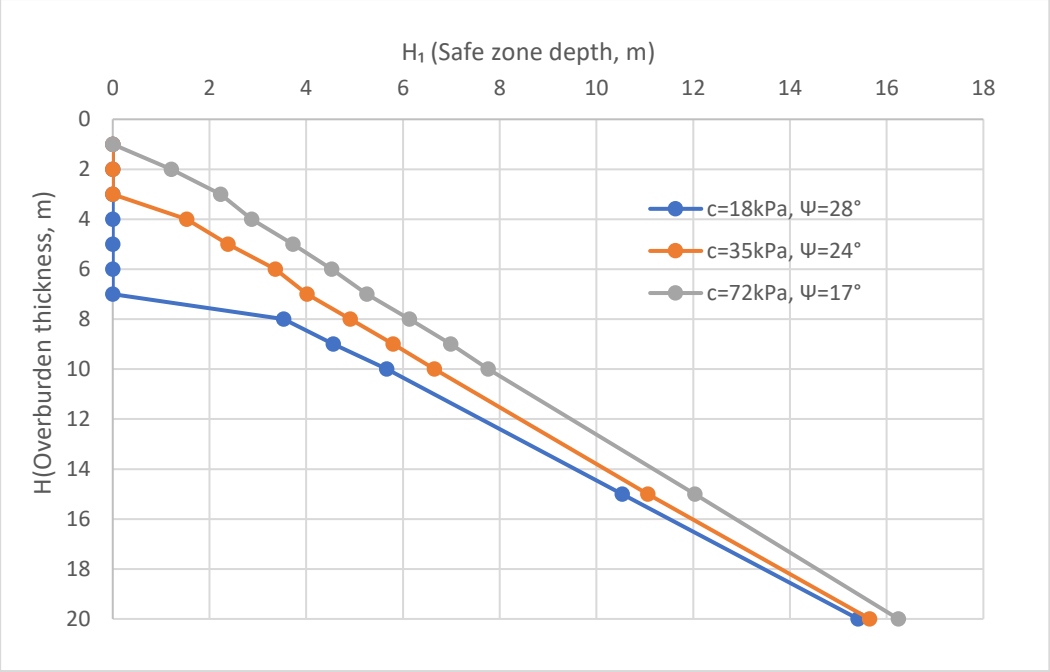


*Figure 4.9* Relationship between $H_1$ and H for 100% saturated cohesive soil with different consistency under fixed dimension scenario

## 4.4 Discussion

In the conducted analysis of the underground cavity within cohesive soil models, several key findings were observed regarding the stability and behavior of the ground surface and cavity by defining the safe zone depth ($H_1$) and maximum weak zone height ($H_2$) around the cavity.

Two general scenarios were taken into consideration for models, one of which is 'Fixed bottom' while the other is 'Fixed dimension'. Within each scenario, the study focused on different soil consistencies and both dry and fully saturated conditions to provide a comprehensive understanding of the factors influencing stability around the void and ground surface.

- Minimum overburden thickness ($H_m$)

Figure 4.10 and Figure 4.11 show the correlation between the minimum overburden thickness for the appearance of safe zone to ensure the stability of ground surface and different consistencies of soil demonstrated by cohesion. Figure 4.10 is for 'Fixed bottom scenario', while 4.11 is for 'Fixed dimension' scenario.

Both dry and saturated conditions show that weaker soils (lower cohesion and higher friction angle) exhibit greater required minimum overburden thickness ($H_m$) to achieve stability (Figure 4.3, Figure 4.5, Figure 4.7 & Figure 4.9). In dry conditions, safe zones form at shallower overburden depth (around 18 m for 'Fixed bottom' & 4 m for 'Fixed dimension') compared to fully saturated conditions (around 22 m for 'Fixed bottom' and 8 m for 'Fixed dimension') for soft soil.

The increase in safe zone depth ($H_1$) with overburden thickness (H) is more rapid in dry condition due to higher effective stress and shear strength (Figure 4.3 & Figure 4.7; Figure 4.5 & Figure 4.9). From Figure 4.10 and Figure 4.11, two minimum stable overburden thickness trendlines converge as the consistency of soil goes higher because of less effects coming from pore water pressure.

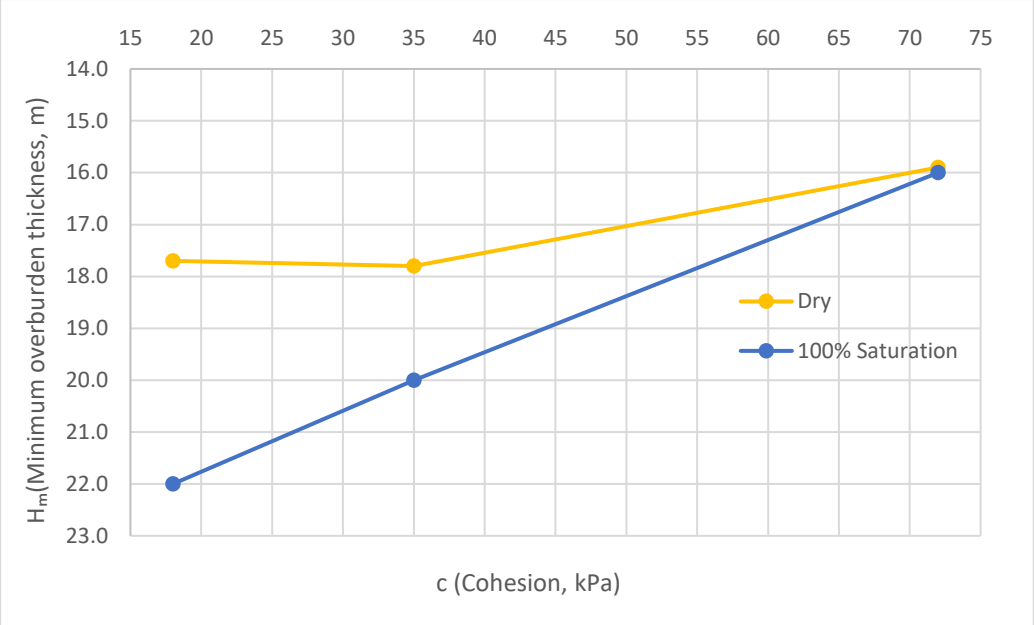


*Figure 4.10* Minimum overburden thickness for stable ground for different cohesion under fixed bottom scenario

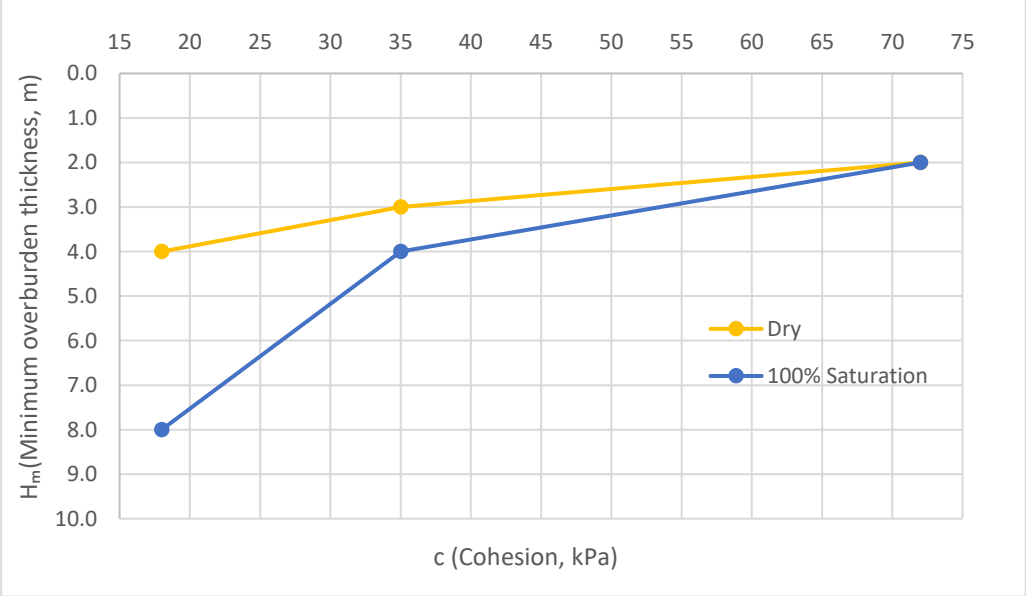


*Figure 4.11* Minimum overburden thickness for stable ground for different cohesion under fixed dimension scenario

- Maximum weak zone height ($H_2$)

The maximum weak zone height ($H_2$) is always greater than the height of the void no matter what scenario or condition was applied, which means a comprehensive reinforcement work should be carried out around the whole void in real situations such as tunnels or mine workings.

## 4.5 Conclusions

The analysis demonstrates the critical role of soil properties, specifically cohesion and friction angle, in determining the stability of the ground above underground voids. Ensuring sufficient overburden thickness is paramount for stabilizing the ground surface, particularly in varying soil consistencies and water conditions. The minimum values to achieve stability of ground surface for dry and fully saturated conditions are 18 m and 22 m under ‘Fixed bottom’ scenario, and 4 m and 8 m under 'Fixed dimension’ scenario, respectively.

By considering both scenarios (Fixed dimension & Fixed bottom), the analyses offer an insight of predicting the potential unstable zone around the void. The maximum weak zone height ($H_2$) is always greater than height of the void.

Both $H_1$ and $H_2$ may also emphasize the need for tailored reinforcement strategies based on specific soil conditions and water content to mitigate risks of ground instability and ensure the safety of structures built over or near underground cavities.

# Chapter 5 Numerical Simulation and Stability Analysis of Underground Cavity in Limestone

This chapter shows an insight into the numerical simulation and stability analysis in limestone. Similar to soil, the modeling scenarios includes both 'Fixed bottom' and 'Fixed dimension' scenarios, different water conditions and limestone qualities defined by GSI values. This chapter seeks to thoroughly evaluate the stability of the ground surface in relation to underground cavities in limestone.

## 5.1 Limestone properties utilized in simulation

General properties such as unit weight and Young's modulus are in their average or intermediate values to simplify the modeling process to focus on the influences of the rock quality. The unit weight of limestone was 23 kN/m$^3$ (Cunningham, 1918). The Young's modulus was 5900000 kPa, and Poisson's ratio was 0.23 (LRFD, 2012). As mentioned by Evert Hoek (2007), the estimated intact compressive strength of limestone was 100 MPa. Gravitational field stress option is selected. According to Sheorey (1994), when depth was 50 m, the horizontal stress ratio $K_o$=1.1. In terms of Terzaghi and Richard (1952), $K_o$=0.3 when Poisson's ratio was to 0.23. And $K_o$=2.7 when depth was 50 m from Arjang and Herget (1997). Therefore, an approximately average value of $K_o$ which was 1.5 has been determined for the model.

Different limestone qualities are of concern in this research. As Hoek-Brown failure criterion was applied to the model, geological strength index (GSI) was introduced to demonstrate the rock surface qualities and joint conditions. When GSI increases, the

interlocking of rock pieces increases, and the surface quality goes from poor to good. In this study, four conditions of limestone with GSI=10, 20, 30 and 50 were selected (Hoek et al, 2013). According to Davarpanah et al (2022), the intact rock constant $m_i$ for limestone was from 5.3 to 14.6. And from Evert Hoek (2007), $m_i$ was 10 ± 2. So, the average value of $m_i$ selected was 10 in the study. Disturbance factor 'D' was set to be 0 (Hoek, 2007).

The effect of blast damage on the near surface rock mass properties is automatically calculated from equation 5, 6 and 7 by the software.

$$m_b = m_i \times e^{\left(\frac{GSI-100}{28-14D}\right)} \quad \text{Equation 5}$$

$$s = e^{\left(\frac{GSI-100}{9-3D}\right)} \quad \text{Equation 6}$$

And

$$a = 0.5 + \frac{1}{6}\left(e^{-GSI/15} - e^{-20/3}\right) \quad \text{Equation 7}$$

Where,

$m_i$ = Intact rock constant

a, s = Coefficient

GSI = Geological Strength Index

D = Disturbance factor

The parameters of all the properties are converted with the units to meet the needs of software are listed in Table 5.1.

*Table 5.1* Limestone Properties

| Material | Unit Weight ($MN/m^3$) | Young's Modulus (MPa) | Poisson's Ratio | Intact Compressive Strength (MPa) | Rock Quality (GSI) | $m_i$ | D |
|---|---|---|---|---|---|---|---|
| Limestone | 0.023 | 5900 | 0.23 | 100 | 10 | 10 | 0 |
| | | | | | 20 | | |
| | | | | | 30 | | |
| | | | | | 50 | | |

## 5.2 Stability analysis under dry condition

### 5.2.1 Fixed bottom

Same as soil, the first scenario for limestone material was keeping the bottom of the cavity at 50 m depth, then changing the height of it. At each situation, $H_1$ and $H_2$ were recorded from observation.

Sixty-one models were built in total. Four sample models are presented in Figure 5.1 to demonstrate the difference between S.F. contours around voids with bottom fixed at 50 m depth, and with different thickness of overburden (5 m, 10 m, 14 m and 17 m) in limestone under dry condition.

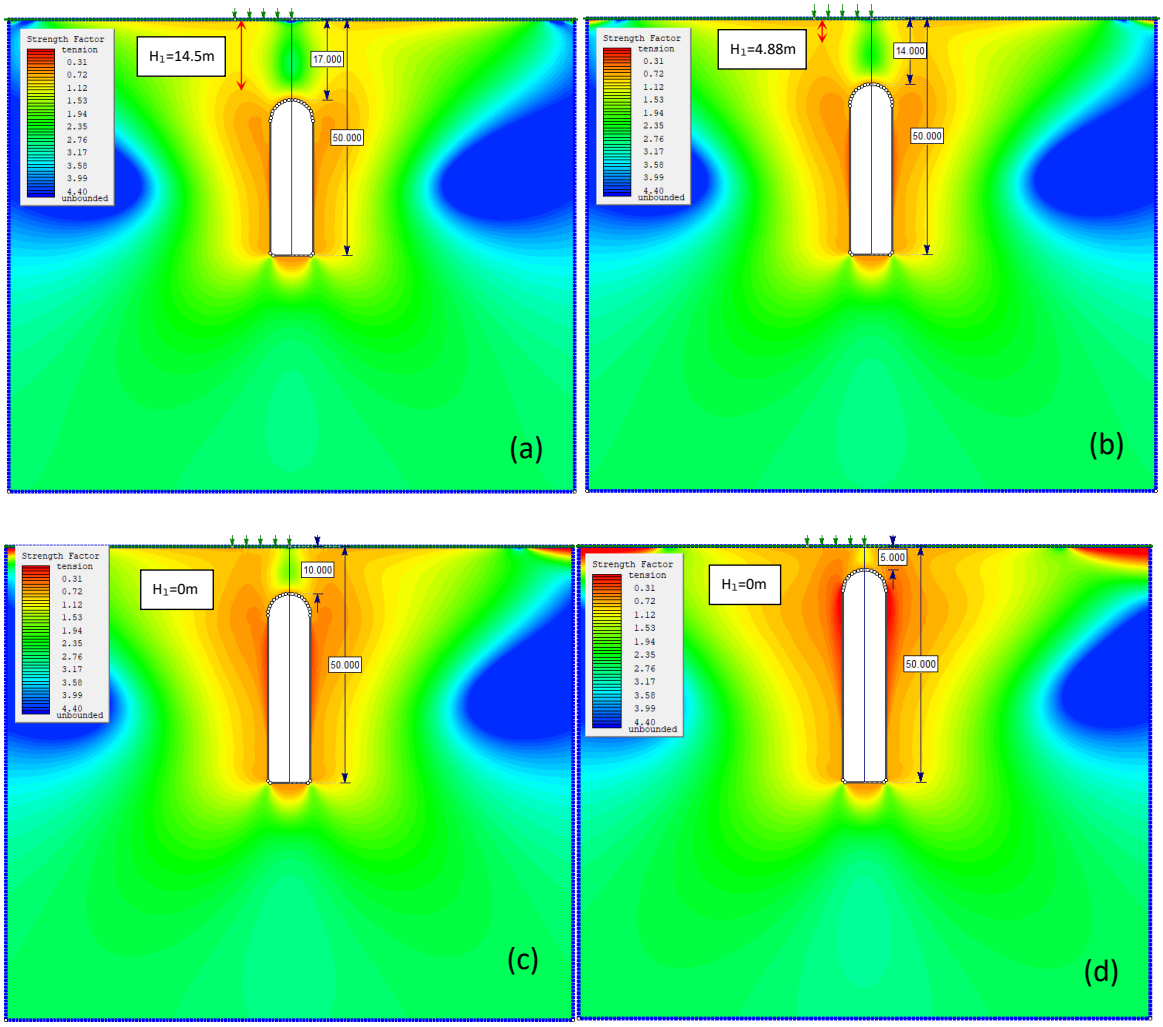


*Figure 5.1* S.F. contour of sample models with fixed bottom in dry limestone when GSI=10: (a)H=17 m; (b)H=14 m; (c)H=10 m; (d)H=5 m

For different conditions of limestone, the ranges of overburden thickness are set to be different to cover all the situations from dangerous zone directly interacting with ground surface to the void deep enough to secure safety of the ground. The observed data are listed in Table 5.2, Table 5.3, Table 5.4 and Table 5.5.

*Table 5.2* Observed $H_1$ and $H_2$ when GSI=10 for dry limestone under fixed bottom scenario

| H(m) | 0.3 | 0.5 | 1 | 2 | 3 | 4 | 5 | 6 | 7 | 8 |
|---|---|---|---|---|---|---|---|---|---|---|
| $H_1$(m) | 0.00 | 0.00 | 0.00 | 0.00 | 0.00 | 0.00 | 0.00 | 0.00 | 0.00 | 0.00 |
| $H_2$(m) | | | | | | | | | | 50.00 |
| H(m) | 9 | 10 | 11 | 12 | 13 | 14 | 15 | 16 | 17 | |
| $H_1$(m) | 0.00 | 0.00 | 0.00 | 0.00 | 0.00 | 4.88 | 9.94 | 12.51 | 14.50 | |
| $H_2$(m) | 49.93 | 49.90 | 49.89 | 49.91 | 49.89 | 44.95 | 39.90 | 37.41 | 35.32 | |

Note: H—Overburden thickness; $H_1$—Safe zone depth; $H_2$—Maximum weak zone height.

*Table 5.3* Observed $H_1$ and $H_2$ when GSI=20 for dry limestone under fixed bottom scenario

| H(m) | 0.3 | 0.5 | 1 | 2 | 3 | 4 | 5 | 6 | 7 | 8 |
|---|---|---|---|---|---|---|---|---|---|---|
| $H_1$(m) | 0.00 | 0.00 | 0.00 | 0.00 | 0.00 | 0.000 | 0.00 | 0.00 | 0.00 | 1.48 |
| $H_2$(m) | 28.13 | 30.39 | 35.00 | 37.71 | 37.40 | 39.15 | 39.14 | 39.65 | 40.00 | 38.40 |
| H(m) | 9 | 10 | 11 | 12 | | | | | | |
| $H_1$(m) | 2.04 | 3.42 | 6.24 | 9.18 | | | | | | |
| $H_2$(m) | 38.04 | 36.82 | 33.96 | 31.11 | | | | | | |

Note: H—Overburden thickness; $H_1$—Safe zone depth; $H_2$—Maximum weak zone height.

*Table 5.4* Observed $H_1$ and $H_2$ when GSI=30 for dry limestone under fixed bottom scenario

| H(m) | 0.3 | 0.5 | 1 | 2 | 3 | 4 | 5 | 6 | 7 | 8 |
|---|---|---|---|---|---|---|---|---|---|---|
| $H_1$(m) | 0.00 | 0.00 | 0.00 | 0.00 | 0.00 | 0.00 | 1.02 | 1.65 | 2.44 | 3.66 |
| $H_2$(m) | 18.53 | 24.88 | 35.59 | 39.21 | 40.26 | 41.16 | 40.35 | 39.76 | 39.02 | 37.78 |
| H(m) | 9 | 10 | 11 | 12 | | | | | | |
| $H_1$(m) | 5.61 | 7.98 | 10.11 | 12.00 | | | | | | |
| $H_2$(m) | 35.92 | 33.93 | 31.82 | 29.87 | | | | | | |

Note: H—Overburden thickness; $H_1$—Safe zone depth; $H_2$—Maximum weak zone height.

*Table 5.5* Observed $H_1$ and $H_2$ when GSI=50 for dry limestone under fixed bottom scenario

| H(m) | 0.3 | 0.5 | 1 | 2 | 3 | 4 | 5 | 6 |
|---|---|---|---|---|---|---|---|---|
| $H_1$(m) | 0.00 | 0.00 | 0.00 | 1.52 | 2.78 | 3.92 | 5.00 | 6.00 |
| $H_2$(m) | 9.86 | 11.27 | 14.39 | 16.19 | 17.09 | 16.83 | 13.83 | 12.42 |

Note: H—Overburden thickness; $H_1$—Safe zone depth; $H_2$—Maximum weak zone height.

Figure 5.2 shows the relationship between safe zone depth ($H_1$) and overburden thickness (H), indicating that all GSI values show a consistent trend of increasing safe zone depth with increasing overburden thickness, but the rate of increase differ based on the GSI.

For the worst scenario which is GSI=10, safe zone appears when thickness of overburden is greater than 13 m. So, to ensure stability of the ground in the first place without considering growth of sinkhole, the overburden thickness must be at least 14 m.

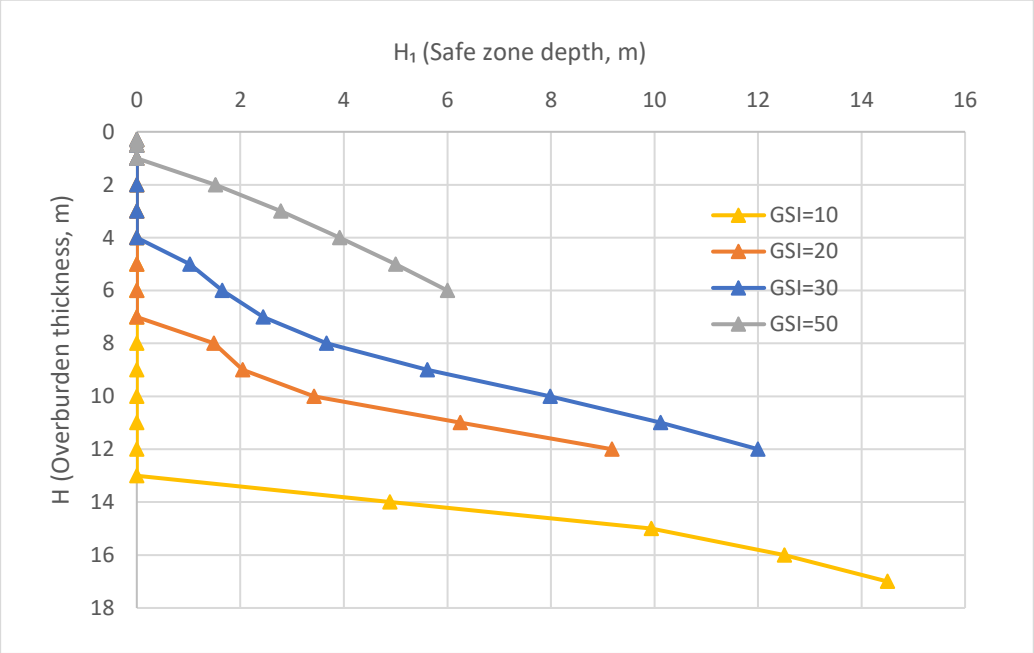


*Figure 5.2* Relationship between $H_1$ and H for dry limestone with different GSI under fixed bottom scenario

Figure 5.3 illustrates the relationship between the maximum weak zone height ($H_2$) and overburden thickness (H) for different limestone quality with different GSI under drained condition. Higher GSI values generally show a more stable behavior with a lower maximum weak zone height at the same overburden thickness. Lower GSI values exhibit

higher maximum weak zone heights on the contrary, indicating greater instability around the void.

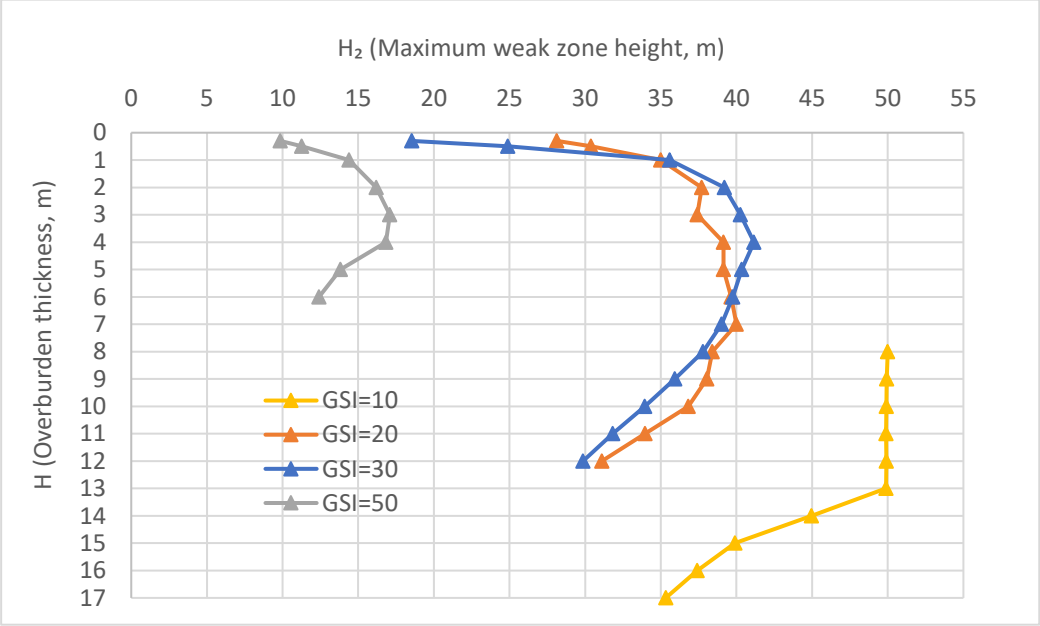


*Figure 5.3* Relationship between $H_2$ and H for dry limestone with different GSI under fixed bottom scenario

$H_2/H_0$ is the ratio of maximum weak zone height to the height of the void. When GSI =10, $H_2/H_0$ is always greater than 1 within the range of overburden thickness studied in Figure 5.4, indicating the instability of the void and necessitated attempts of reinforcement.

For GSI =20, 30 and 50, though the curves exhibit lower values of weak zone height ($H_2$) at shallower depths, it does not represent relatively stable situations. Because the safe zone has not yet showed up, the weak zone is intersecting with ground surface. And the confining pressure concentrates to the upper part of the void and the unstable zone with strength factor lower than 1 stops above the bottom of the void, which results in the lower ratio of $H_2/H_0$.

After certain depth where safe zone shows up, appropriate reinforcement could be introduced to stabilize the void considering the possibility of stabilization when $H_2/H_0$ is smaller than 1.

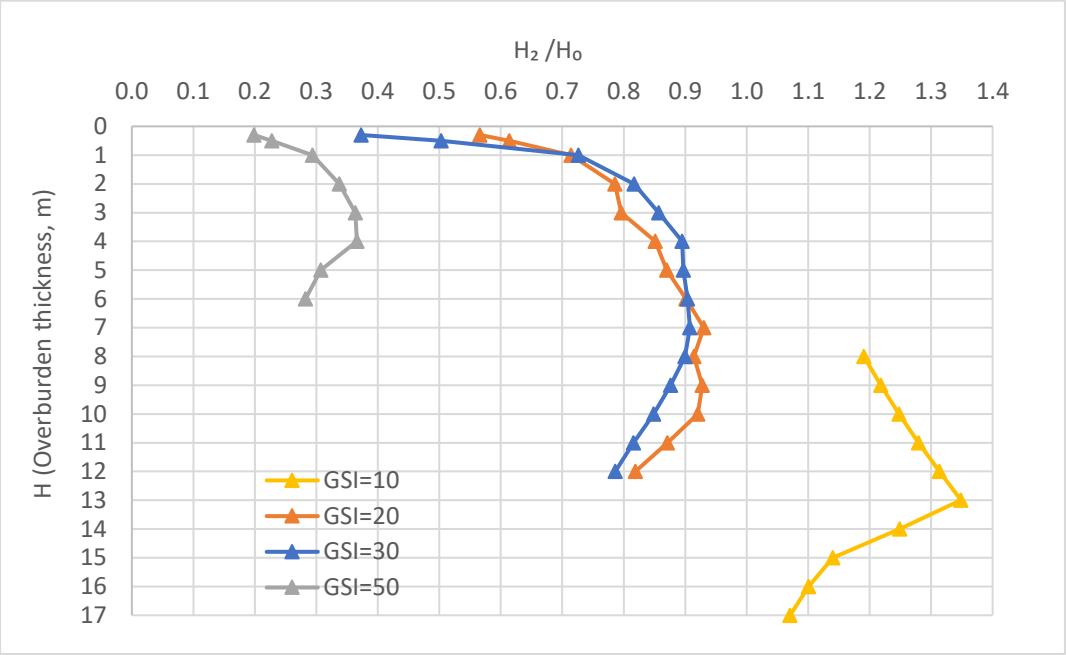


*Figure 5.4* Relationship between $H_2/H_0$ ratio and H for dry limestone with different GSI under fixed bottom scenario

### 5.2.2 Fixed dimension

In this scenario, same to the concept of soil, fixed dimension was applied to the cavity with $H_0$=10 m and $W_0$=9 m. The thickness of overburden was modified to get different S.F. contours around the void along with groups of $H_1$ and $H_2$. The range of overburden thickness H varied from 0.5 m to 10 m.

Thirty-seven models were built in total. Four sample models with GSI=10 are shown in Figure 5.5. The cavities are located 1 m, 2 m, 5 m, and 10 m below the ground surface respectively. As shown in Figure 5.5(c) and Figure 5.5(d), when overburden thickness is 1

m and 2 m, there is a gap zone without S.F. contour displayed between ground surface and cavity. That is an output error area due to the limitation of the software.

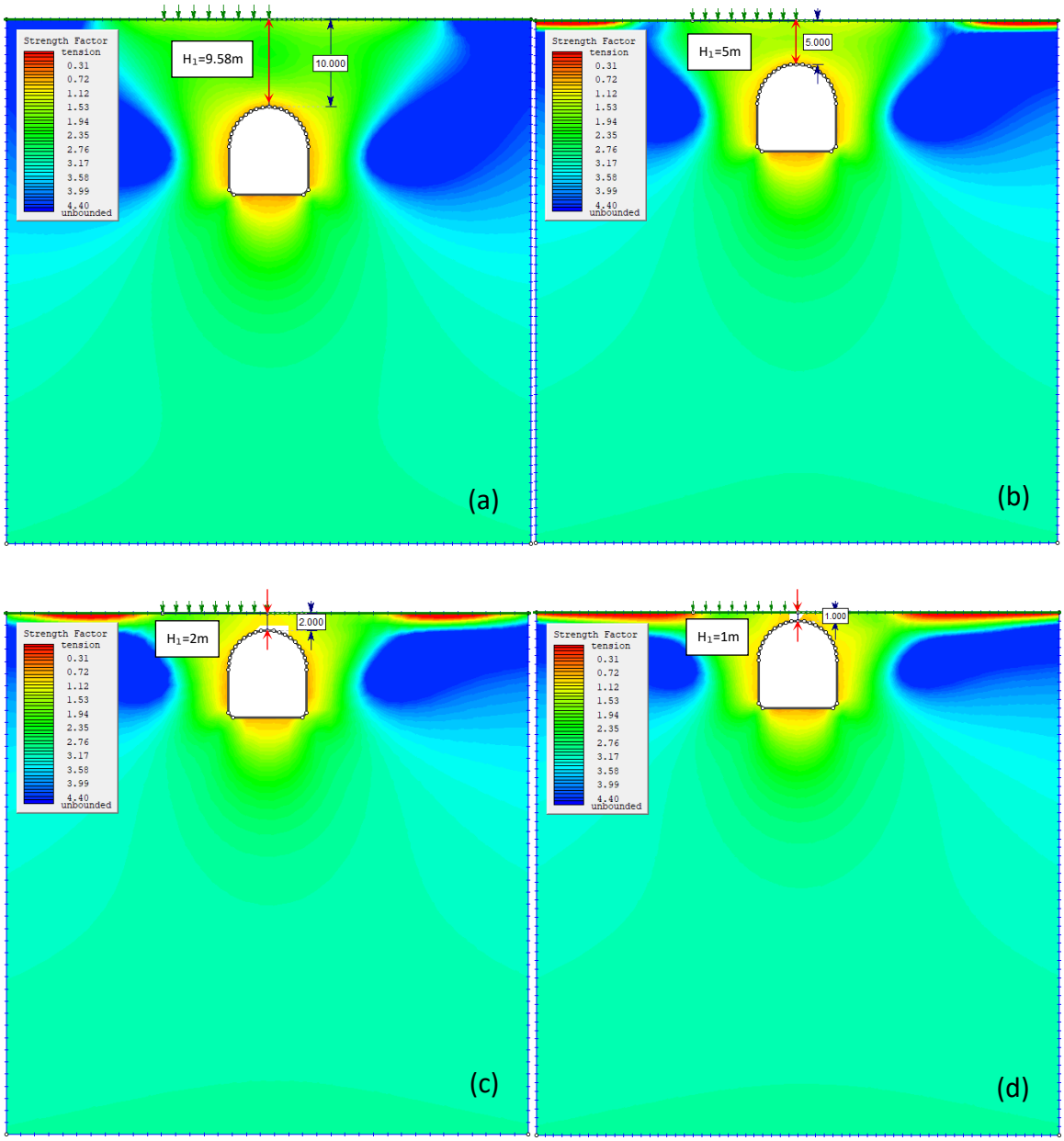


*Figure 5.5* S.F. contour of sample models with fixed dimension in dry limestone when GSI=10: (a)H=10 m; (b)H=5 m; (c)H=2 m; (d)H=1 m

The observed data when GSI equals to 10, 20 and 30 are listed in Table 5.6, Table 5.7 and Table 5.8, respectively. There are no data for the case with GSI=50 because, as shown in

Table 5,8 and Figure 5.6, a safe zone appears when the overburden thickness is greater than 1 meter at GSI=30. However, no data were observed for overburden thickness less than 1 meter. Therefore, if GSI is greater than 30, $H_1$ equals to H at some point when H is less than 1 m. And in real situations, data observed from when GSI=30 are good enough to cover cases with better limestone conditions (GSI>30).

*Table 5.6* Observed $H_1$ and $H_2$ when GSI=10 for dry limestone under fixed dimension scenario

| H(m) | 0.5 | 1 | 2 | 3 | 4 | 5 | 6 | 7 | 8 |
|---|---|---|---|---|---|---|---|---|---|
| $H_1$(m) | | 1.00 | 2.00 | 3.00 | 4.00 | 5.00 | 5.74 | 7.00 | 7.64 |
| $H_2$(m) | | 9.03 | 6.74 | 9.23 | 6.60 | 8.46 | 6.71 | 8.60 | 9.05 |
| H(m) | 9 | 10 | | | | | | | |
| $H_1$(m) | 9.00 | 9.58 | | | | | | | |
| $H_2$(m) | 8.09 | 9.13 | | | | | | | |

Note: H—Overburden thickness; $H_1$—Safe zone depth; $H_2$—Maximum weak zone height.

*Table 5.7* Observed $H_1$ and $H_2$ when GSI=20 for dry limestone under fixed dimension scenario

| H(m) | 0.5 | 1 | 2 | 3 | 4 | 5 | 6 | 7 | 8 |
|---|---|---|---|---|---|---|---|---|---|
| $H_1$(m) | | 0.63 | 1.57 | 2.77 | 4.00 | 5.00 | 6.00 | 7.00 | 8.00 |
| $H_2$(m) | | 4.04 | 4.30 | 6.02 | 5.25 | 7.05 | 5.99 | 7.72 | 6.39 |
| H(m) | 9 | 10 | | | | | | | |
| $H_1$(m) | 9.00 | 10.00 | | | | | | | |
| $H_2$(m) | 6.68 | 6.63 | | | | | | | |

Note: H—Overburden thickness; $H_1$—Safe zone depth; $H_2$—Maximum weak zone height.

*Table 5.8* Observed $H_1$ and $H_2$ when GSI=30 for dry limestone under fixed dimension scenario

| H(m) | 0.5 | 1 | 2 | 3 | 4 | 5 | 6 | 7 | 8 |
|---|---|---|---|---|---|---|---|---|---|
| $H_1$(m) | | 1.00 | 2.00 | 3.00 | 4.00 | 5.00 | 6.00 | 7.00 | 8.00 |
| $H_2$(m) | 0.57 | 1.21 | 1.44 | 2.18 | 2.75 | 3.42 | 3.65 | 5.88 | 4.23 |
| H(m) | 9 | 10 | | | | | | | |
| $H_1$(m) | 9.00 | 10.00 | | | | | | | |
| $H_2$(m) | 4.51 | 4.28 | | | | | | | |

Note: H—Overburden thickness; $H_1$—Safe zone depth; $H_2$—Maximum weak zone height.

Basically, safe zone depth and overburden thickness experience a linear relationship (Figure 5.6). As the overburden thickness increases, the safe zone depth increases linearly for all GSI values. The trendlines converge at H=4 m, after that, the stable zone depth equals to the thickness of overburden. And the similarity across different GSI values suggests that the influence of rock strength (as presented by GSI) on the rate of increase in safe zone depth is minimal.

Considering the most fractured situation with highly weathered surface for limestone (GSI=10), overburden thickness is supposed to be greater than 1 m to ensure the safety of ground surface for the best estimation due to limitation of the software.

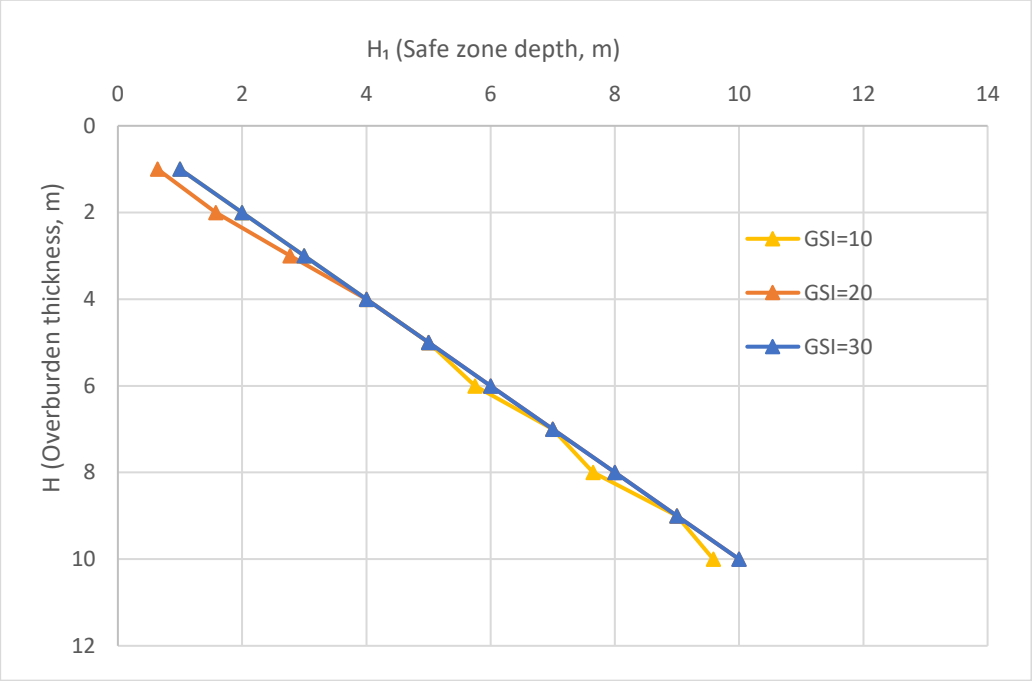


*Figure 5.6* Relationship between $H_1$ and H for dry limestone with different GSI under fixed dimension scenario

As shown in Figure 5.7, lower GSI values result in larger weak zone heights, indicating more extensive vertical instability around the void, while higher GSI values correspond to smaller weak zone heights, indicating more localized vertical instability.

Since given that the height of void is fixed at 10 m under fixed dimension scenario, all the observed weak zone heights are smaller than the void height, especially for higher GSI values. The introduction of reinforcement system is feasible and weaker rocks (lower GSI) necessitate more robust supports due to larger weak zone height.

The interaction between void geometry and the overburden stress can lead to non-linear stress distribution patterns, resulting in fluctuation weak zone heights. Also, in weaker limestones (lower GSI), the weak zone height show more pronounced fluctuations due to the rock's inability to uniformly distribute stresses (Hoek, 1994). Another reason is as can be seen in Figure 5.5, bias may exist while defining the unstable area around the void, which may cause the fluctuation as well.


*Figure 5.7* Relationship between $H_2$ and H for dry limestone with different GSI under fixed dimension scenario

## 5.3 Stability analysis under fully saturated condition

### 5.3.1 Fixed bottom

Forty-nine models were built in total. Figure 5.8 shows four sample models when GSI =10 under fully saturated water condition. The thicknesses of overburden are 40 m, 30 m, 20 m and 14 m while bottom of the void is fixed at 50 m depth below ground surface. Different color contours represent different strength factors.

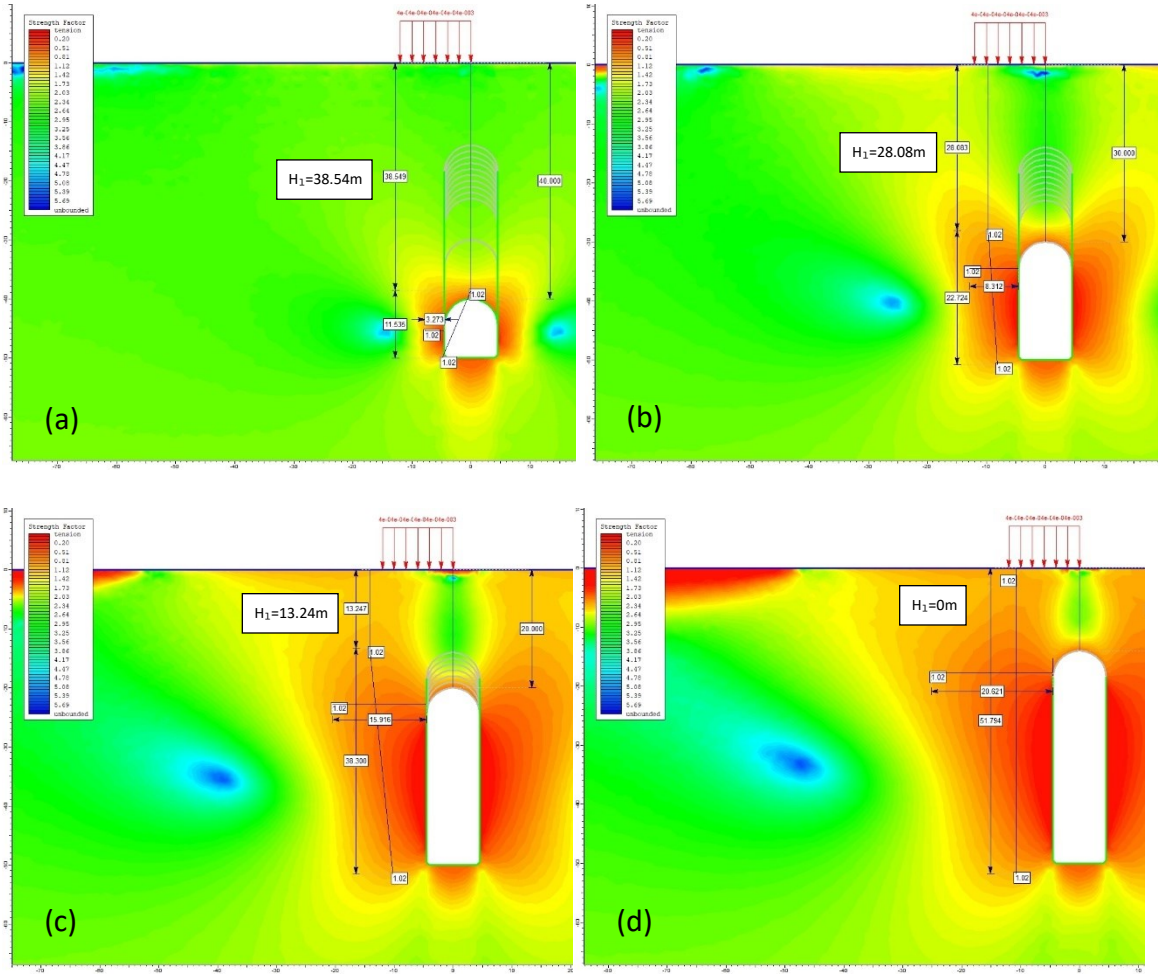


*Figure 5.8* S.F. contour of sample models with fixed bottom in fully saturated limestone when GSI=10: (a)H=40 m; (b)H=30 m; (c)H=20 m; (d)H=14 m

Data observed for saturated limestone when GSI =10, 20, 30 and 50 are recorded in Table 5.9, Table 5.10, Table 5.11 and Table 5.12, respectively.

*Table 5.9* Observed $H_1$ and $H_2$ when GSI=10 for 100% saturated limestone under fixed bottom scenario

| H(m) | 14 | 15 | 16 | 17 | 18 | 19 | 20 | 21 | 22 |
|---|---|---|---|---|---|---|---|---|---|
| $H_1$(m) | 0.00 | 0.00 | 3.25 | 6.66 | 9.08 | 11.29 | 13.24 | 14.85 | 16.51 |
| $H_2$(m) | 51.79 | 51.82 | 48.59 | 44.90 | 42.43 | 40.35 | 38.30 | 36.62 | 34.88 |
| H(m) | 23 | 30 | 40 | | | | | | |
| $H_1$(m) | 18.01 | 28.08 | 38.54 | | | | | | |
| $H_2$(m) | 33.27 | 22.72 | 11.53 | | | | | | |

Note: H—Overburden thickness; $H_1$—Safe zone depth; $H_2$—Maximum weak zone height.

*Table 5.10* Observed $H_1$ and $H_2$ when GSI=20 for 100% saturated limestone under fixed bottom scenario

| H(m) | 9 | 10 | 11 | 12 | 13 | 14 | 15 | 16 | 17 |
|---|---|---|---|---|---|---|---|---|---|
| $H_1$(m) | 0.00 | 0.00 | 2.15 | 3.34 | 4.91 | 6.52 | 8.38 | 10.28 | 11.60 |
| $H_2$(m) | 50.56 | 50.56 | 48.40 | 47.21 | 45.64 | 44.04 | 42.17 | 40.28 | 38.95 |
| H(m) | 18 | 19 | 30 | 40 | | | | | |
| $H_1$(m) | 13.29 | 14.57 | 29.57 | 39.03 | | | | | |
| $H_2$(m) | 37.26 | 35.98 | 20.44 | 10.93 | | | | | |

Note: H—Overburden thickness; $H_1$—Safe zone depth; $H_2$—Maximum weak zone height.

*Table 5.11* Observed $H_1$ and $H_2$ when GSI=30 for 100% saturated limestone under fixed bottom scenario

| H(m) | 4 | 5 | 6 | 7 | 8 | 9 | 10 | 11 | 12 |
|---|---|---|---|---|---|---|---|---|---|
| $H_1$(m) | 0.00 | 0.00 | 1.40 | 2.09 | 2.58 | 3.50 | 4.63 | 6.04 | 7.46 |
| $H_2$(m) | 49.84 | 48.71 | 48.44 | 47.75 | 47.26 | 46.34 | 45.21 | 43.86 | 42.44 |
| H(m) | 20 | 30 | 40 | | | | | | |
| $H_1$(m) | 18.04 | 29.42 | 39.22 | | | | | | |
| $H_2$(m) | 31.75 | 20.29 | 10.41 | | | | | | |

Note: H—Overburden thickness; $H_1$—Safe zone depth; $H_2$—Maximum weak zone height.

*Table 5.12* Observed $H_1$ and $H_2$ when GSI=50 for 100% saturated limestone under fixed bottom scenario

| H(m) | 1 | 2 | 3 | 4 | 5 | 6 | 7 | 8 | 10 |
|---|---|---|---|---|---|---|---|---|---|
| $H_1$(m) | 0.00 | 2.000 | 3.000 | 4.00 | 5.00 | 6.00 | 7.00 | 8.00 | 10.00 |
| $H_2$(m) | 48.85 | 46.08 | 43.22 | 41.35 | 39.55 | 38.07 | 36.36 | 34.62 | 48.85 |
| H(m) | 20 | 30 | 40 | | | | | | |
| $H_1$(m) | 20.00 | 30.00 | 39.65 | | | | | | |
| $H_2$(m) | 25.97 | 17.3 | 9.51 | | | | | | |

Note: H—Overburden thickness; $H_1$—Safe zone depth; $H_2$—Maximum weak zone height.

Figure 5.9 shows the relationship between the safe zone depth ($H_1$) and overburden thickness (H) for different limestone quality with different GSI under fully saturated condition. All GSI values exhibit a consistent trend of increasing safe zone depth with increasing overburden thickness, but the rate of increase differs based on GSI values,

where higher GSI experiences higher rate. Also, stronger rock (higher GSI) has higher safe zone and vice versa when looking at the same overburden depth.

The minimum safe zone depth to stabilize the ground surface with consideration of sinkhole growth is 16 m.

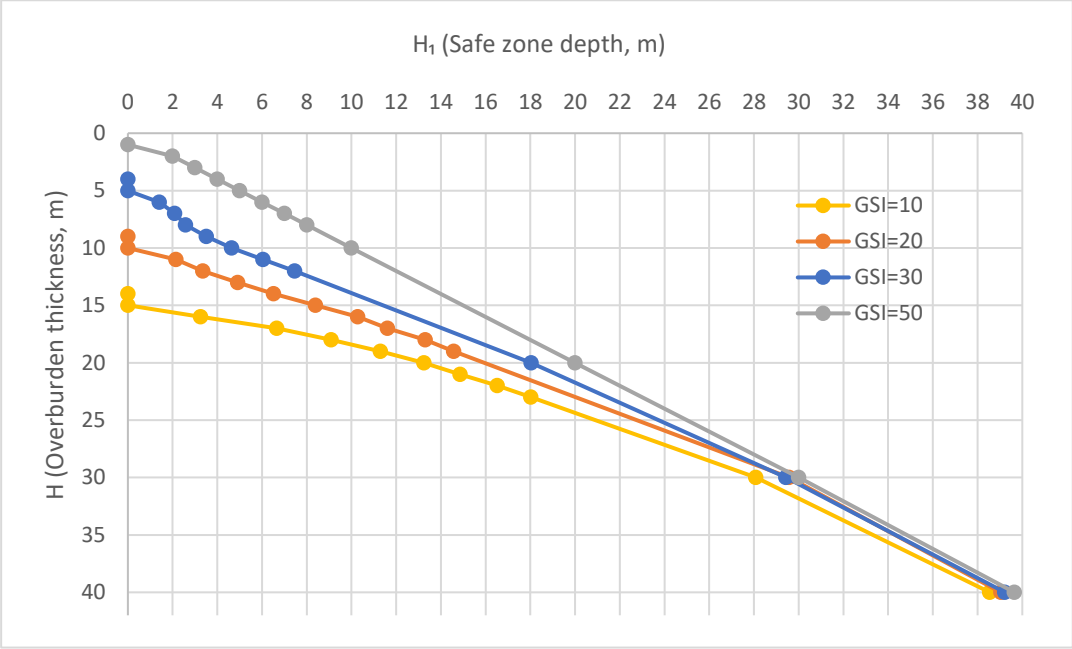


*Figure 5.9* Relationship between $H_1$ and H for 100% saturated limestone with different GSI under fixed bottom scenario

Figure 5.10 illustrates the relationship between the maximum weak zone width ($H_2$) and overburden thickness (H) for different limestone quality with different GSI Fully saturated condition. Higher GSI values generally show a more stable behavior with a lower maximum weak zone height at the same overburden thickness. On the other hand, lower GSI values exhibit higher maximum weak zone heights, indicating greater instability around the void.

All correlations are negative, which means maximum weak zone height decreases as the void getting shorter, though at different rates based on GSI.

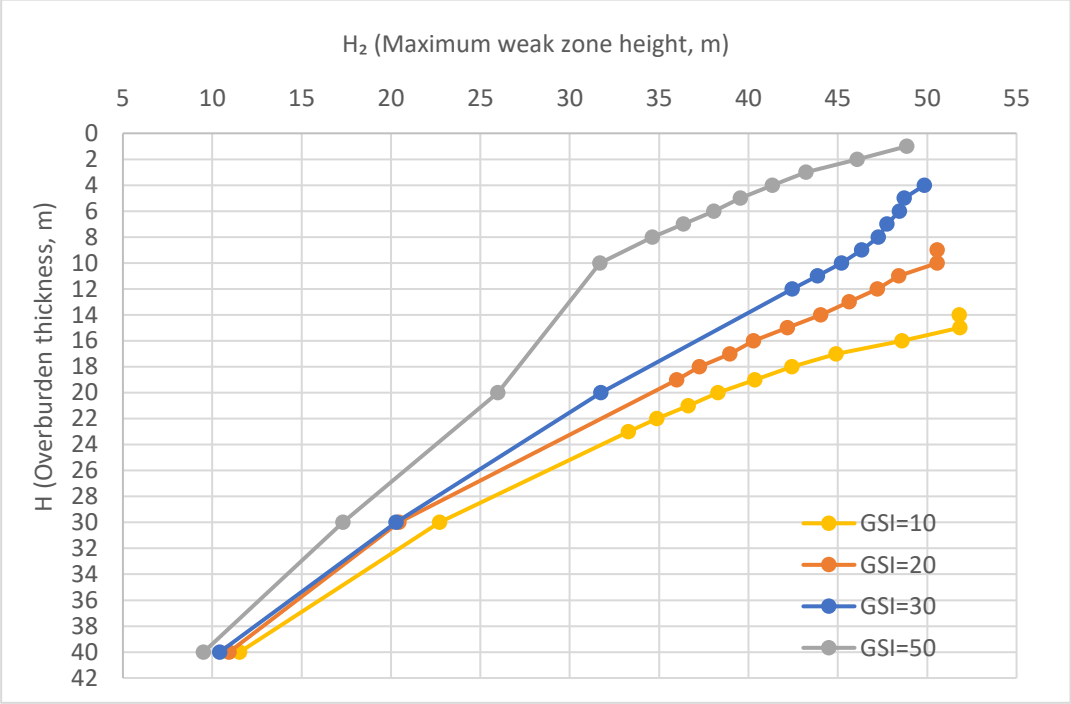


*Figure 5.10* Relationship between $H_2$ and H for 100% saturated limestone with different GSI under fixed bottom scenario

Figure 5.11 gives direct view to the ratio of maximum weak zone height over thickness of overburden ($^{H_2}/_{H_0}$). For GSI values equal to 10, 20 and 30, the ratios are always greater than 1, indicating the void is surrounded by unstable rocks. For GSI =50, $^{H_2}/_{H_0}$ does not exceed 1, which suggest that part of the rock is unstable.

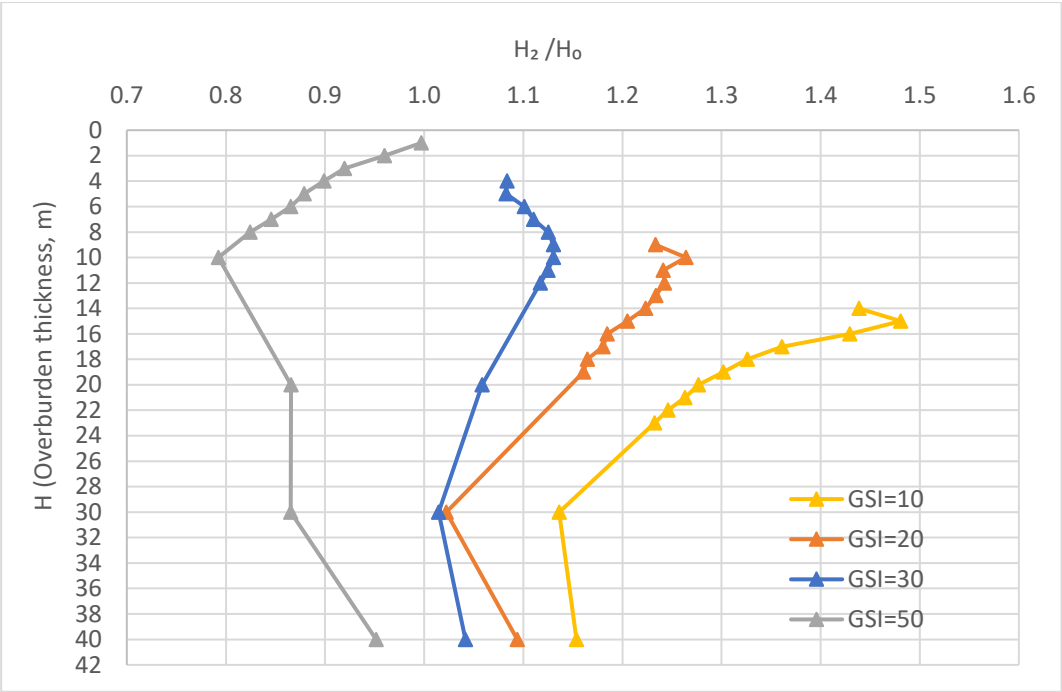


*Figure 5.11* Relationship between $H_2/H_o$ ratio and H for 100% saturated limestone with different surface conditions under fixed bottom scenario

### 5.3.2 Fixed dimension

Thirty-three fully saturated limestone models were built in total. Four samples when GSI equals to 10 are shown below in Figure 5.12. Under fixed dimension scenario, $H_o$ is 9 m and $W_o$ is 10 m. Overburden thickness in sample models are 15 m, 10 m, 5 m and 1 m, respectively.

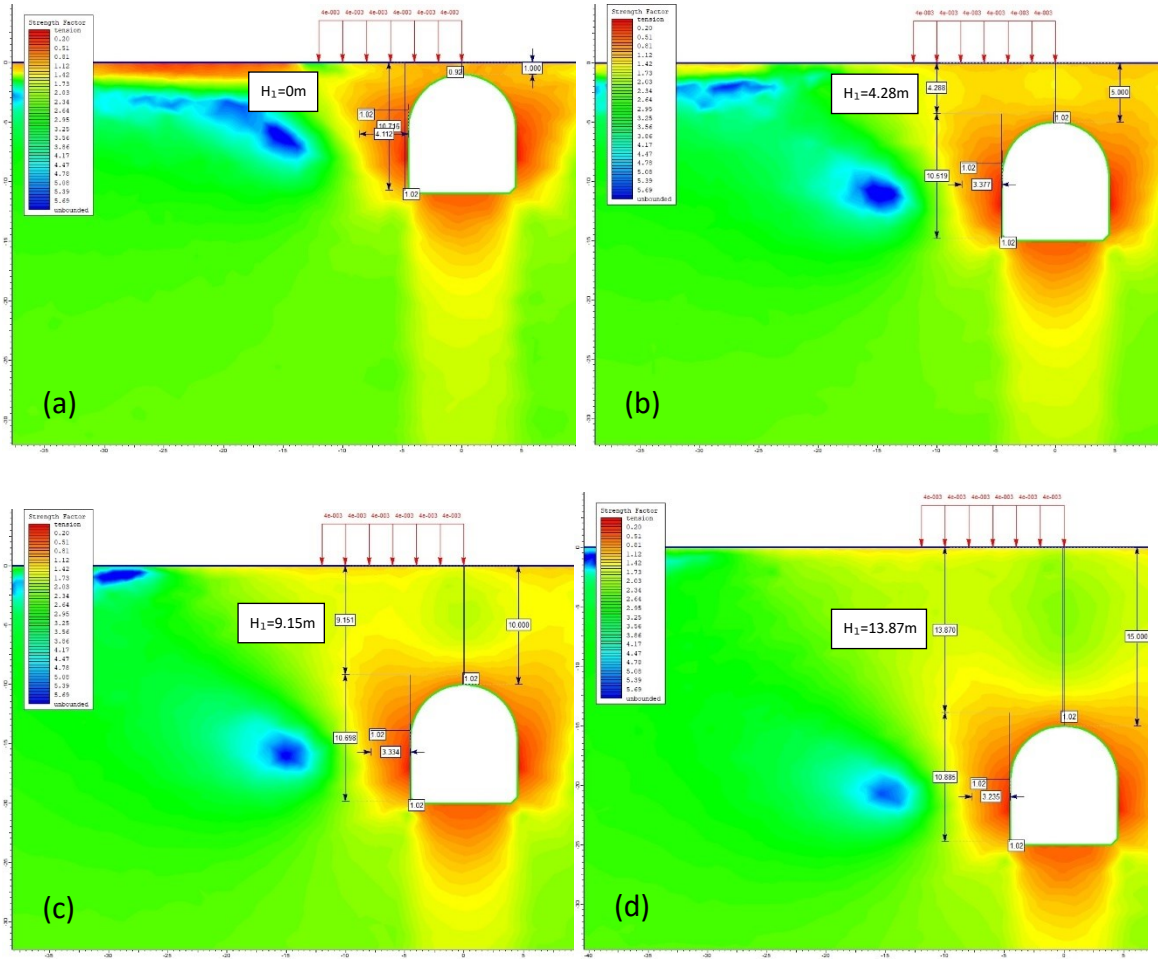


*Figure 5.12* S.F. contour of sample models with fixed dimension in fully saturated limestone when GSI=10: (a)H=1 m; (b)H=5 m; (c)H=10 m; (d)H=15 m

Same as dry condition, models with GSI =30 are significant that safe zone appears when overburden thickness < 1 m. The objective is reached, thus, there is no need of data for GSI =50 to represent better conditions.

The observed data are collected and listed in Table 5.13, Table 5.14 and Table 5.15 for fully saturated limestone models with GSI =10, 20 and 30.

*Table 5.13* Observed $H_1$ and $H_2$ when GSI=10 for 100% saturated limestone under fixed dimension scenario

| H(m) | 1 | 2 | 3 | 4 | 5 | 6 | 7 | 8 | 9 |
|---|---|---|---|---|---|---|---|---|---|
| $H_1$(m) | 0.00 | 1.49 | 2.45 | 3.41 | 4.28 | 5.28 | 6.22 | 7.14 | 8.17 |
| $H_2$(m) | 10.71 | 10.17 | 10.30 | 10.32 | 10.51 | 10.50 | 10.56 | 10.81 | 10.51 |
| H(m) | 10 | 15 | | | | | | | |
| $H_1$(m) | 9.15 | 13.87 | | | | | | | |
| $H_2$(m) | 10.69 | 10.88 | | | | | | | |

Note: H—Overburden thickness; $H_1$—Safe zone depth; $H_2$—Maximum weak zone height.

*Table 5.14* Observed $H_1$ and $H_2$ when GSI=20 for 100% saturated limestone under fixed dimension scenario

| H(m) | 1 | 2 | 3 | 4 | 5 | 6 | 7 | 8 | 9 |
|---|---|---|---|---|---|---|---|---|---|
| $H_1$(m) | 0.00 | 1.84 | 2.68 | 3.68 | 4.58 | 5.56 | 6.53 | 7.57 | 8.42 |
| $H_2$(m) | 10.55 | 9.56 | 9.83 | 9.82 | 10.05 | 10.06 | 10.08 | 10.07 | 10.07 |
| H(m) | 10 | 15 | | | | | | | |
| $H_1$(m) | 9.40 | 14.31 | | | | | | | |
| $H_2$(m) | 10.19 | 10.14 | | | | | | | |

Note: H—Overburden thickness; $H_1$—Safe zone depth; $H_2$—Maximum weak zone height.

*Table 5.15* Observed $H_1$ and $H_2$ when GSI=30 for 100% saturated limestone under fixed dimension scenario

| H(m) | 1 | 2 | 3 | 4 | 5 | 6 | 7 | 8 | 9 |
|---|---|---|---|---|---|---|---|---|---|
| $H_1$(m) | 1.00 | 2.00 | 3.00 | 4.00 | 5.00 | 6.00 | 6.78 | 7.75 | 8.69 |
| $H_2$(m) | 5.25 | 5.82 | 6.86 | 7.58 | 7.94 | 8.88 | 9.75 | 9.74 | 9.45 |
| H(m) | 10 | 15 | | | | | | | |
| $H_1$(m) | 9.64 | 14.57 | | | | | | | |
| $H_2$(m) | 9.74 | 9.66 | | | | | | | |

Note: H—Overburden thickness; $H_1$—Safe zone depth; $H_2$—Maximum weak zone height.

Compared to dry condition, Figure 5.13 shows the same correlations between safe zone depth ($H_1$) and overburden thickness (H). Also, stronger rock with higher GSI values experiences larger safe zone depth considering the same overburden thickness.

The only difference is that the presence of water increases pore water pressure, which may reduce effective stresses and thus the shear strength of the material, leading to the

increase of minimum overburden thickness for the stability of ground surface. And the minimum overburden thickness is 2 m.

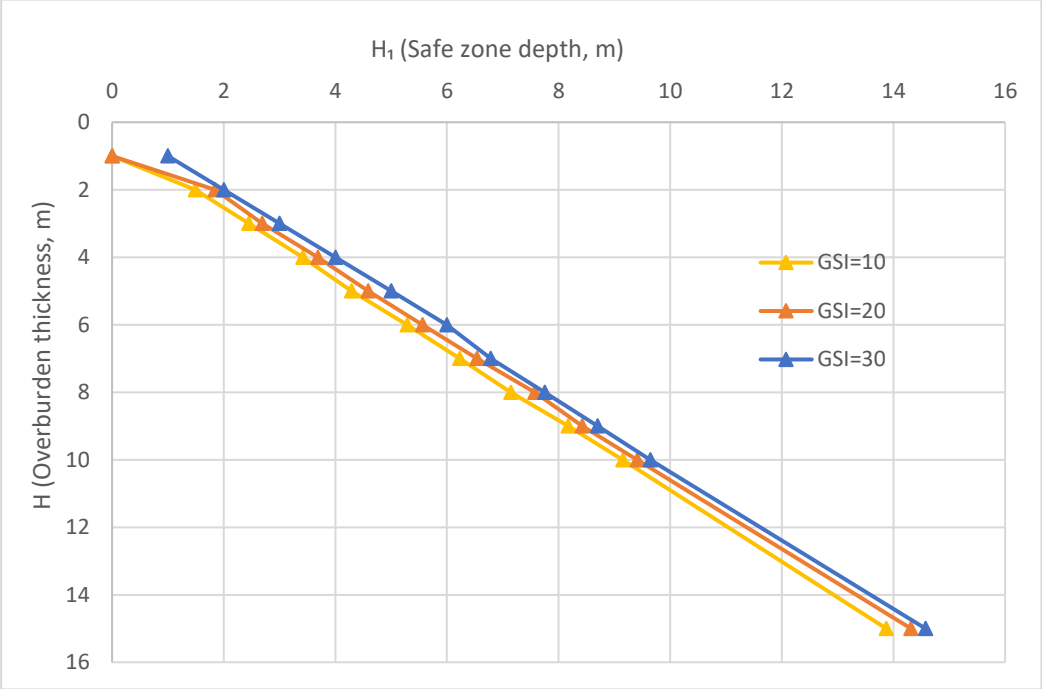


*Figure 5.13* Relationship between $H_1$ and H for 100% saturated limestone with different GSI under fixed dimension scenario

Figure 5.14 exhibits the relationship between maximum weak zone height ($H_2$) and overburden thickness (H) for GSI =10, 20 and 30 respectively under fully saturated condition. Lower GSI values lead to greater weak zone heights, signifying more extensive vertical instability around the void, whereas higher GSI values correspond to smaller weak zone heights, indicating more localized vertical instability.

For GSI =10 and 20, there are no big changes of maximum weak zone heights as overburden thickness increases. However, due to the participation of pore water pressure, the increase rate is significant for GSI =30 when overburden thickness is less than 7 m.

When more than 7 m, the trendlines associated with different GSI values show similar behavior.

For fixed dimension scenario, the height of void is fixed at 10 m, so $H_2$ is always smaller for GSI =30 and always bigger for GSI =10. For GSI =20, the ratio $H_2/H_0$ fluctuates around 1 depending on the location of the void. Therefore, less reinforcement attempts are needed for stronger rocks (higher GSI values).

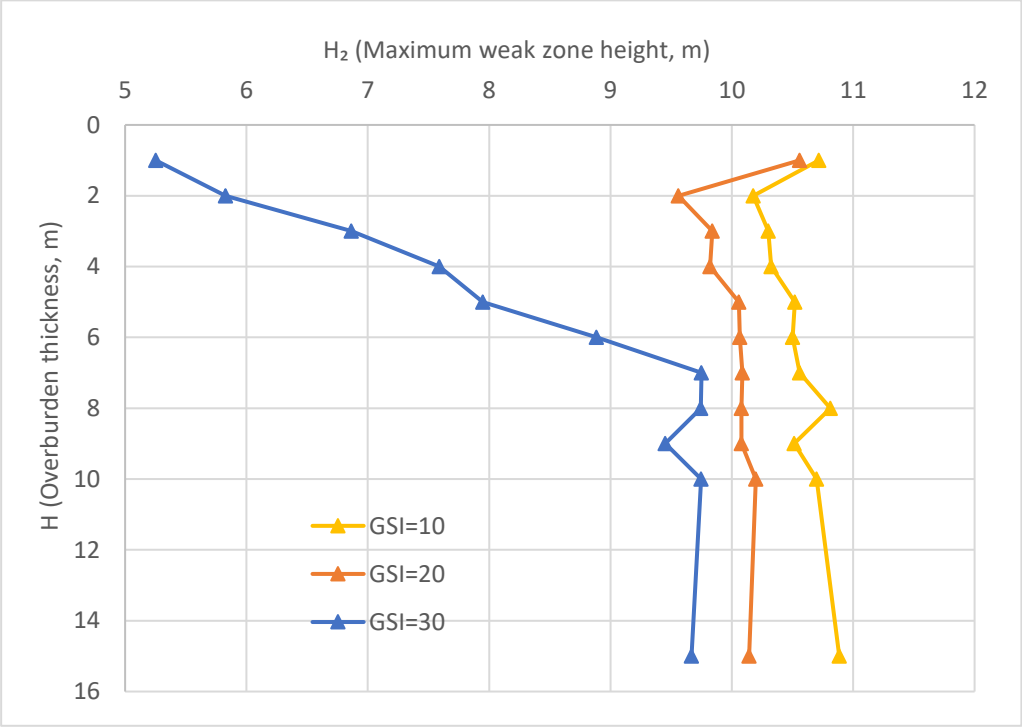


*Figure 5.14* Relationship between $H_2$ and H for 100% saturated limestone with different GSI under fixed dimension scenario

## 5.4 Discussion

Similar to soil, the stability analysis of underground cavity within limestone models under both dry and fully saturated water conditions reveals several critical insights regarding the

behavior and reinforcement needs of the whole structure. Key findings may vary from the 'Fixed bottom' and 'Fixed dimension' scenarios across different rock qualities interpreted by Geological Strength Index (GSI) values.

- Minimum overburden thickness ($H_m$)

Figure 5.15 and Figure 5.16 show the relationship between the minimum overburden thickness for the appearance of safe zone to ensure the stability of ground surface and different limestone qualities demonstrated by GSI.

In both dry and fully saturated conditions, the safe zone depth ($H_1$) increases with overburden thickness (H). However, the required minimum overburden thickness for the formation of safe zones is higher in fully saturated conditions. For instance, in fully saturated conditions, safe zones begin to appear at around 16 m for 'Fixed bottom' scenario and 2 m for 'Fixed dimension' scenario. Whereas, in dry conditions, they are around 14 m and 1 m for each scenario, respectively.

Higher GSI values (indicating better limestone quality) lead to more stable conditions with lower safe zone depth (Figure 5.2, Figure 5.6, Figure 5.9 and Figure 5.13). The increase of material strength results in the convergence of trendlines in Figure 5.15 and Figure5.16 as GSI increases.

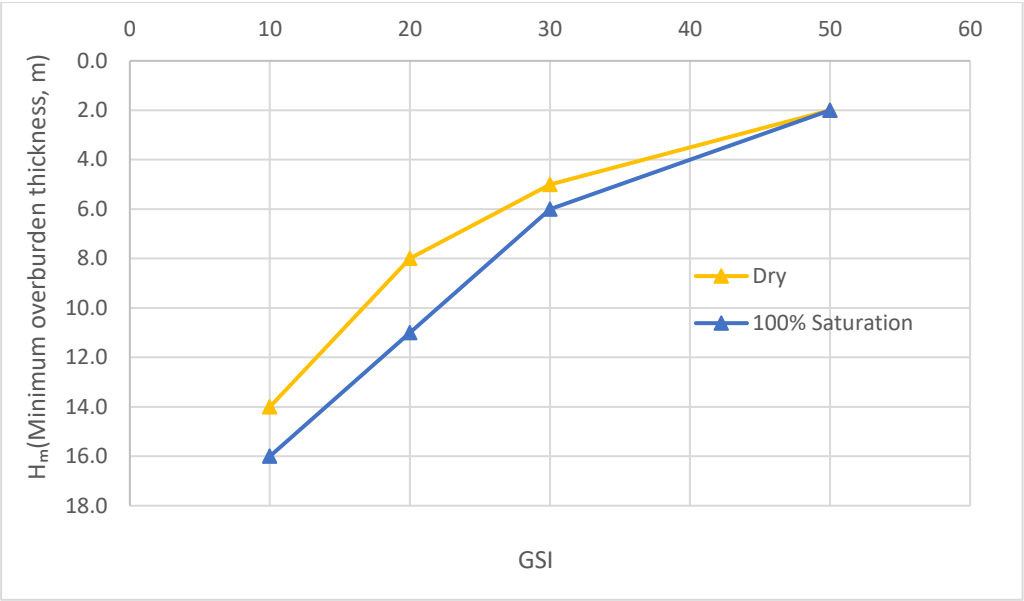


*Figure 5.15* Minimum overburden thickness for stable ground for different GSI under fixed bottom scenario

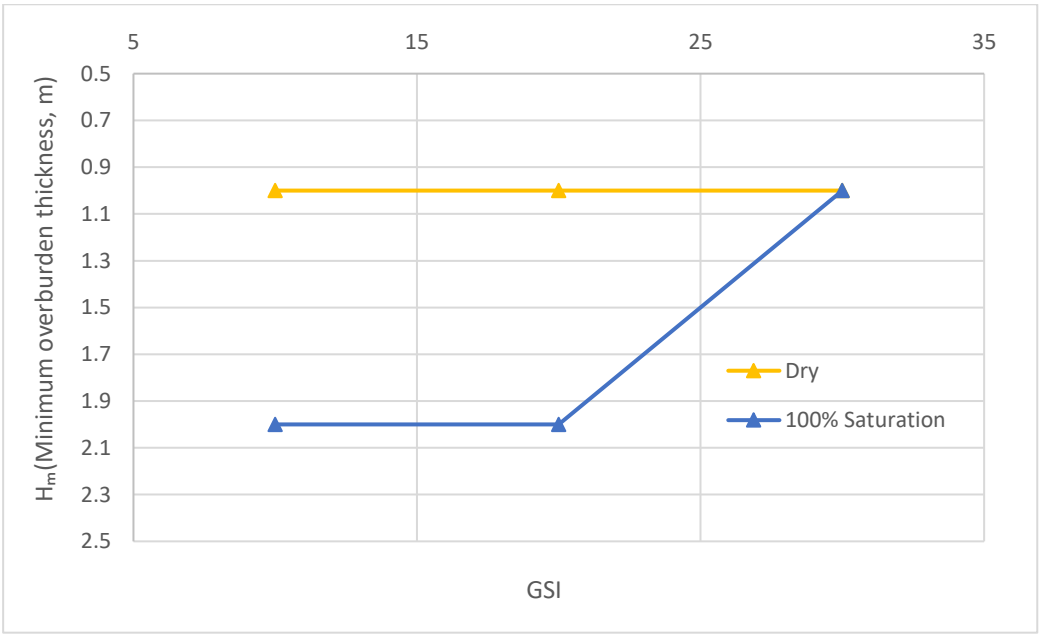


*Figure 5.16* Minimum overburden thickness for stable ground for different GSI under fixed dimension scenario

- Maximum weak zone height ($H_2$)

Fully saturated conditions result in higher maximum weak zone heights compared to dry conditions. The additional pore water pressure reduces effective stresses, leading to greater vertical instability (Figure 5.4 and Figure 5.11; Figure 5.7 and Figure 5.14). Also, for both scenarios, lower GSI values (weaker limestone) exhibit larger weak zone height at the same overburden thickness and vice versa.

By looking at the factor maximum weak zone height ($H_2$), it is the ratio $H_2/H_0$ that of concern which indicates how big portion of boundary alone side the cavity is unstable. If the ratio is greater 1, then the whole void is within unstable situation, which requires more robust reinforcement than when $H_2/H_0 < 1$.

## 5.5 Conclusions

The Geological Strength Index (GSI) and water content are critical factors influencing the stability of underground cavities. Higher GSI values correlate with increased stability, while the presence of water significantly reduces stability, requiring more comprehensive reinforcement. Therefore, to ensure stability, the overburden thickness must be greater in fully saturated conditions compared to dry conditions. Because the presence of water significantly decreases the strength of the material. The values for dry and fully saturated conditions are 14 m and 16 m under 'Fixed bottom' scenario, meanwhile, 1 m and 2 m for 'Fixed dimension' scenario, respectively.

Besides the factors mentioned above, the influenced unstable area is also affected by the size and location of the void considering both scenarios.

Same to concept from soil, tailored reinforcement or water drainage strategies are essential, particularly in fully saturated conditions and weaker limestone (lower GSI) where weak zones are broader. These strategies should consider the specific geological conditions and potential water content to guarantee the safety of structures built over or near underground cavities.

# Chapter 6 Conclusions and Recommendations

## 6.1 Conclusions

This study aims to analyze the stability of the overburden above underground cavities in cohesive soil and limestone using numerical modeling under varying conditions (dry and fully saturated) and scenarios ('Fixed bottom' & 'Fixed dimension') by considering the ground stability defined by strength factor. Several key findings have been identified and summarized below.

1) Modeling scenarios

Both 'Fixed bottom' and 'Fixed dimension' scenarios provide insights into the different factors influencing ground stability. The 'Fixed bottom' scenario shows more rapid increases in safe zone depth with overburden thickness due to the decrease of the cavity height, while the 'Fixed dimension' scenario highlights the importance of cavity locations. The data generated from all the models could be used as reference for the assessment of ground stability above natural cavities, tunnels, mine workings, etc. in real situations.

2) Influence of soil and limestone properties

The stability of underground cavities is significantly influenced by soil and limestone properties, particularly cohesion and friction angle for soil and Geological Strength Index (GSI) for limestone in this research, which defines the quality of the soil and limestone, respectively. Weaker materials exhibit larger unstable zones and require greater overburden thickness to achieve stability.

For soil under ‘Fixed bottom’ scenario, the minimum overburden thickness required to achieve the stability of the ground surface decreases from 22 m to 16 m under dry conditions and 18 m to 16 m under fully saturated conditions, as the cohesion increases from 18 kPa to 72 kPa. In the ‘Fixed dimension’ scenario, the minimum overburden thickness decreases from 8 m to 2 m under dry conditions and 4 m to 2 m under fully saturated conditions, as the cohesion increases from 18 kPa to 72 kPa.

For limestone under ‘Fixed bottom’ scenario, the minimum overburden thickness required to achieve the stability of the ground surface decreases from 16 m to 2 m under dry conditions and 14 m to 2 m under fully saturated conditions, as the GSI value increases from 10 to 50. In the ‘Fixed dimension’ scenario, the minimum overburden thickness decreases from 2 m to 1 m under dry conditions and remains at 1 m under fully saturated conditions, as the GSI value increases from 10 to 30.

3) Impact of water content

The presence of water significantly reduces the stability of both soil and limestone by increasing pore water pressure and decreasing shear strength. With fully saturated water condition, the minimum overburden thickness for stable ground decreases by 4 m for weaker soil under both ‘Fixed bottom’ and ‘Fixed dimension’ scenarios. The value drops by 2 m and 1 m for limestone under ‘Fixed bottom’ and ‘Fixed dimension’ scenarios, respectively. This necessitates more comprehensive water drainage strategies in fully saturated condition to mitigate risks of ground stability.

4) Minimum overburden thickness to maintain stability of ground surface

The minimum overburden thickness is the most important indicator when determining the stability of ground surface.

Cohesive Soil with lower cohesion and higher friction angles require greater overburden thickness (H) to achieve stability as mentioned earlier. Fully saturated water condition necessitate a greater overburden thickness to ensure ground surface stability due to reduced shear strength from pore water pressure. So, the minimum values of overburden thickness for dry and 100% saturated conditions are 18 m and 22 m under 'Fixed bottom' scenario, and 4 m and 8 m under 'Fixed dimension' scenario, respectively.

Similar trends were observed in limestone models, where higher GSI values correlated with increased stability and lower safe zone depths. Likewise, the minimum values of overburden thickness for dry and 100% saturated conditions are 14 m and 16 m under 'Fixed bottom' scenario, and 1 m and 2 m under 'Fixed dimension' scenario, respectively.

In general, for cohesive soil, the minimum overburden thickness to achieve the stability of ground surface for dry and fully saturated conditions are 18 m and 22 m under 'Fixed bottom' scenario, and 4 m and 8 m under 'Fixed dimension' scenario, respectively. For limestone, the minimum overburden thickness for dry and fully saturated conditions are 14 m and 16 m under 'Fixed bottom' scenario, and 1 m and 2 m under 'Fixed dimension' scenario, respectively.

5) Variation of weak zone

The maximum height of weak zone ($H_2$) around the cavity varies with different material properties and water conditions. Though for soil, the maximum weak zone height ($H_2$) is always greater than the void height ($H_o$), suggesting the needs of more robust reinforcements.

Weaker materials and saturated conditions result in larger weak zones, indicating more extensive instability. Also, the unstable zone around the void provides a perspective of the potential growth of the sinkhole.

## 6.2 Recommendations

Possible errors include approximation of modeling itself and interpretation inaccuracies of the modeling results, particularly in some of the cases when the void is close to the ground surface, and errors from manually selected data. Therefore, it is not recommended to reference these results before calibration.

Future works may focus on two aspects. The first one is extending the modeling scenarios to include more realistic geological settings and different types of underground cavities to provide a more comprehensive understanding of the factors influencing stability. In addition, integrate data from real-world sinkhole events to validate and refine these models, providing better predictive capabilities for future occurrences.

Second, due to the limitations of the software, only static analysis was generated during the research. So, the other research direction could be using more functional numerical modeling software to simulate the progression of sinkholes over time.

# References


Aliabadi, F. M. (2020). Boundary element methods. In Encyclopedia of continuum mechanics. Berlin, Heidelberg: Springer Berlin Heidelberg. (pp. 182-193)

Arjang, B., & Herget, G. (1997). In situ ground stresses in the Canadian hard rock mines: an update. International Journal of Rock Mechanics and Mining Sciences, 34(3-4), 15-e1.

Augarde, C. E., Lyamin, A. V., & Sloan, S. W. (2003). Prediction of undrained sinkhole collapse. Journal of Geotechnical and Geoenvironmental Engineering, 129(3). 197-205.

Bowles, J. E. (1977). Foundation analysis and design (2nd edition). New York: McGraw-Hill. (pp. 86)

Bowles, J. E. (1997). Foundation analysis and design (5th edition). New York: McGraw-Hill. (pp. 123, 163)

Butterfield, R. (1999). Dimensional analysis for geotechnical engineers. Geotechnique, 49(3), 357-366.

Cunningham, B. (1918). A treatise on the principles and practice of harbour engineering. Griffin. (pp. 86)

COE, U. A. (1990). Engineering and design, settlement analysis. Engineering Manual No. 1110-1-1904. (pp. D-5)

Davarpanah, S. M., Sharghi, M., Vásárhelyi, B., & Török, Á. (2022). Characterization of Hoek–Brown constant mi of quasi-isotropic intact rock using rigidity index approach. Acta Geotechnica, 17(3), 877-902.

de Sousa Oliveira, L., Maia, R. N., de Assis Júnior, R. N., Romero, R. E., Costa, M. C. G., de Alencar, T. L., & Mota, J. C. A. (2020). Tensile strength values for the degrees of soil consistency using human perception and TS-Soil device. Catena, 190, 104541.

Fang, H. Y., & Hirst, T. J. (1973). A method for determining the strength parameters of soils. Highway Research Record, (463).

Groud, G. J. A. (1951). The precise topographical measurements in coal mine underground works. Proc. Int. Conf. Rock Pressure and Support in Workings, Liege, 52-66.

Groud, G. J. A. (1957). Ground movement due to mining with different types of strata and at different depths. Proc. European Congress on Ground Movement, 115-125.

Hoek, E., Carranza-Torres, C., & Corkum, B. (2002). Hoek-Brown failure criterion-2002 edition. Proceedings of NARMS-Tac, 1(1), 267-273.

Hoek, E., Carter, T. G., & Diederichs, M. S. (2013, June). Quantification of the geological strength index chart. In ARMA US Rock Mechanics/Geomechanics Symposium (pp. ARMA-2013). ARMA.

Hoek, E. (1994). Strength of rock and rock masse. News journal of international society for rock mechanics, 2(2), 4-16.

Hoek, E. (2007). Practical rock engineering. 2007. Online. ed. Rocscience.

Hudson, J. A., & Harrison, J. P. (2000). Engineering rock mechanics: an introduction to the principles. Elsevier.

Knappett, J., & Craig, R. F. (2019). Craig's Soil Mechanics (9th edition). CRC Press.

Lamb, B., & Shiau, J. (2014). A physical and numerical investigation into sinkhole formation. In Fourth International Conference on Geotechnique, Construction Materials and Environment, Brisbane, Australia (pp. 1-6).

LRFD, AASHTO. (2012). Bridge design specifications. American Association of State Highway and Transportation Officials, AASHTO: Washington, DC, USA. (pp. (10-25) – (10 - 27))

Memmott, M. (2013, March 1). Sinkhole swallows sleeping man in Florida. NPR. https:// www.npr.org/sections/thetwo-way/2013/03/01/173225027/sinkhole-swallows-sleeping -man-in-florida

Mirza Hassan, M. (2019). Numerical investigation of sinkhole stability in undrained clay (Doctoral dissertation, University of Southern Queensland).

Morel, L. C. (2013, May 24). Documents reveal more details in Seffner sinkhole. Tampa B ay News. https://www.tampabay.com/news/publicsafety/documents-reveal-more-detai ls-in-seffner-sinkhole/2122576/

NCB. (1950-51). Memorandum on design of mine workings to secure effective strata control. Divisional Strata Control Research Committee, Durham and Northern (N&C) Divisions, National Coal Board. Trans. I. Mine. E., 110, 251-265.

Reddish, D. J., & Whittaker, B. N. (2012). Subsidence: occurrence, prediction and control. Elsevier.

Rocscience. (n.d.). Gravity Field Stress (Tutorial). Retrieve from: https://www.rocscience.com/help/rs2/documentation/rs2-model/loading/field-stress/gravity-field-stress

Ruth, B. E., Beggs, T. F., & Degner, J. D. (1985). Predicting sinkhole collapse. Civil Engineering—ASCE, 55(11), 58-60.

Sheorey, P. R. (1994, February). A theory for in situ stresses in isotropic and transversely isotropic rock. In International journal of rock mechanics and mining sciences & geomechanics abstracts (Vol. 31, No. 1, pp. 23-34). Pergamon.

Shiau, J., Keawsawasvong, S., Chudal, B., Mahalingasivam, K., & Seehavong, S. (2021). Sinkhole stability in elliptical cavity under collapse and blowout conditions. Geosciences, 11(10), 421.

Siddharthan, R., Norris, G., & Edil, T. (1992). "Effect of Overburden Pressure on Shear Strength Parameters." Journal of Geotechnical Engineering, ASCE, Vol. 118, No. 5, pp. 740-757.

Sowers, G. F. (1996, June). Building on sinkholes: design and construction of foundations in karst terrain. American Society of Civil Engineers.

TALEB, H. A., & GUEMIDI, I. (2023). Studied the Impact of the Foundation on the Underground Cavity Using the Finite Element Method. Journal of Science, Technology and Engineering Research, 4(1), 9-16.

Terzaghi, K., Peck, R. B., & Mesri, G. (1996). Soil mechanics in engineering practice (3rd edition). John wiley & sons. (pp. 63)

Terzaghi, K., & Richart, F. E. (1952). Stresses in rock about cavities. Geotechnique. 3:57-90

Whittaker, B.N., & Pye, J.H. (1975, September). Design and layout aspects of longwall methods of coal mining. In ARMA US Rock Mechanics/Geomechanics Symposium (pp. ARMA-75). ARMA.

Whittaker, B. N., Reddish, D. J. & Fitzpatrick, D. J. (1985). Calculation by computer program of mining subsidence ground strata patterns due to multiple longwall extractions. Mine Science and Technology, 3, 21-33.

Wilson, W. L. (1995). Sinkhole and buried sinkhole densities and new sinkhole frequencies of Northwest Peninsular Florida. In Proc., 5th Mult. Conf., Sinkholes (pp. 79-97).

# Appendices

## Appendix A --- Chapter 4 Referencing tables and figures for soil properties

*Table A- 1* Empirical values for Φ, $D_r$, and unite weight of granular soils based on the SPT at about 6 m depth and normally consolidated (Bowles, 1997)

| Description | Very loose | Loose | Medium | Dense | Very dense |
|---|---|---|---|---|---|
| Relatively density $D_r$ | 0 | 0.15 | 0.35 | 0.65 | 0.85 |
| SPT $N'_{70}$: fine<br>medium<br>coarse | 1-2<br>2-3<br>3-6 | 3-6<br>4-7<br>5-9 | 7-15<br>8-20<br>10-25 | 16-30<br>21-40<br>26-45 | ?<br>>40<br>>45 |
| Φ: fine<br>medium<br>coarse | 26-28<br>27-38<br>28-30 | 28-30<br>30-32<br>30-34 | 30-34<br>32-36<br>33-40 | 33-38<br>36-42<br>40-50 | <50 |
| γ, kN/m³ | 11-16 | 14-18 | 17-20 | 17-22 | 20-23 |

*Table A- 2* Values or value ranges for Poisson's ratio ν (Bowles, 1997)

| Type of soil | ν |
|---|---|
| Clay, saturated | 0.4-0.5 |
| Clay, unsaturated | 0.1-0.3 |
| Sandy clay | 0.2-0.3 |
| Silt | 0.3-0.35 |
| Sand, gravelly sand | -0.1-1 |
| commonly used | 0.3-0.4 |
| Rock | 0.1-0.4 (depends somewhat on type of rock) |
| Loess | 0.1-0.3 |
| Ice | 0.36 |
| Concrete | 0.15 |
| Steel | 0.33 |

*Table A- 3* Typical elastic moduli (COE, 1990)

| Soil | $E_s$ (tsf) |
|---|---|
| Clay | |
| Very soft clay | 5-50 |
| Soft clay | 50-200 |
| Medium clay | 200-500 |
| Stiff clay, silty clay | 500-1000 |
| Sandy clay | 250-2000 |
| Clay shale | 1000-2000 |
| | |
| Sand | |
| Loose sand | 100-250 |
| Dense sand | 250-1000 |
| Dense sand and gravel | 1000-2000 |
| Silty sand | 250-2000 |

*Table A- 4* Relation of consistency of clay, number of blows $N_{60}$ on sampling spoon, and unconfined compressive strength (Terzaghi, 1996)

| | $q_u$ (kPa) | | | | | |
|---|---|---|---|---|---|---|
| Consistency | Very soft | Soft | Medium | Stiff | Very stiff | Hard |
| $\mathrm{N}_{60}$ | <2 | 2-4 | 4-8 | 8-15 | 15-30 | >30 |
| $q_u$ | <25 | 25-50 | 50-100 | 100-200 | 200-400 | >400 |

*Table A- 5* Selected strength properties (drained, laboratory-scale) for soils (Ortiz et al., 1986)

| | Cohesion (kPa) | Friction angle | |
|---|---|---|---|
| | | Peak (°) | Residual (°) |
| gravel | ----- | 34 | 32 |
| sandy gravel with few fines | ----- | 35 | 32 |
| sandy gravel with silty or clayey fines | 1.0 | 35 | 32 |
| mixture of gravel and sand with fines | 3.0 | 28 | 22 |
| uniform sand --- fine | ----- | 32 | 30 |
| uniform sand --- coarse | ----- | 34 | 30 |
| well-graded sand | ----- | 33 | 32 |
| low-plasticity silt | 2.0 | 28 | 25 |
| medium to high-plasticity silt | 3.0 | 25 | 22 |
| low-plasticity clay | 6.0 | 24 | 20 |
| medium-plasticity clay | 8.0 | 20 | 10 |
| high-plasticity clay | 10.0 | 17 | 6 |
| organic silt of clay | 7.0 | 20 | 15 |

*Table A- 6* Typical values of Coefficient of Earth Pressure at Rest, $K_o$ (Rocscience, n.d.)

| No. | Soil Type | $K_o$ |
|---|---|---|
| 1 | Dense sand | 0.35 |
| 2 | Loose sand | 0.6 |
| 3 | Normally consolidated clays | 0.5-0.6 |
| 4 | lightly overconsolidated clays | 1 |
| 5 | Heavily overconsolidated clays | 3 |

## Appendix B --- Chapter 5 Referencing tables and figures for limestone properties

*Table B - 1* Summary of elastic moduli for intact rock (LRFD, 2012)

| Rock type | No. of values | No. of rock types | Elastic modulus, $E_s$ (ksi*10³) | | | Standard deviation (ksi*10³) |
|---|---|---|---|---|---|---|
| | | | Maximum | Minimum | Mean | |
| Granite | 26 | 26 | 14.5 | 0.93 | 7.64 | 3.55 |
| Diorite | 3 | 3 | 16.2 | 2.48 | 7.45 | 6.19 |
| Gabbro | 3 | 3 | 12.2 | 9.80 | 11.0 | 0.97 |
| Diabase | 7 | 7 | 15.1 | 10.0 | 12.8 | 1.78 |
| Basalt | 12 | 12 | 12.2 | 4.20 | 8.14 | 2.60 |
| Quartzite | 7 | 7 | 12.8 | 5.29 | 9.59 | 2.32 |
| Marble | 14 | 13 | 10.7 | 0.58 | 6.18 | 3.49 |
| Gneiss | 13 | 13 | 11.9 | 4.13 | 8.86 | 2.31 |
| Slate | 11 | 2 | 3.79 | 0.35 | 1.39 | 0.96 |
| Schist | 13 | 12 | 10.0 | 0.86 | 4.97 | 3.18 |
| Phyllite | 3 | 3 | 2.51 | 1.25 | 1.71 | 0.57 |
| Sandstone | 27 | 19 | 5.68 | 0.09 | 2.13 | 1.19 |
| Siltstone | 5 | 5 | 4.76 | 0.38 | 2.39 | 1.65 |
| Shale | 30 | 14 | 5.60 | 0.001 | 1.42 | 1.45 |
| Limestone | 30 | 20 | 13.0 | 0.65 | 5.7 | 3.73 |
| Dolostone | 17 | 16 | 11.4 | 0.83 | 4.22 | 3.44 |

*Table B - 2* Summary of Poisson's ratio for intact rock (LRFD, 2012)

| Rock type | No. of values | No. of rock types | Poisson's ratio, v | | | Standard deviation |
|---|---|---|---|---|---|---|
| | | | Maximum | Minimum | Mean | |
| Granite | 22 | 22 | 0.39 | 0.09 | 0.20 | 0.08 |
| Gabbro | 3 | 3 | 0.20 | 0.16 | 0.18 | 0.02 |
| Diabase | 6 | 6 | 0.38 | 0.20 | 0.29 | 0.06 |
| Basalt | 11 | 11 | 0.32 | 0.16 | 0.23 | 0.05 |
| Quartzite | 6 | 6 | 0.22 | 0.08 | 0.15 | 0.05 |
| Marble | 5 | 5 | 0.40 | 0.17 | 0.28 | 0.08 |
| Gneiss | 11 | 11 | 0.40 | 0.09 | 0.22 | 0.09 |
| Schist | 12 | 11 | 0.31 | 0.02 | 0.12 | 0.08 |
| Sandstone | 12 | 9 | 0.46 | 0.08 | 0.20 | 0.11 |
| Siltstone | 3 | 3 | 0.23 | 0.09 | 0.18 | 0.06 |
| Shale | 3 | 3 | 0.18 | 0.03 | 0.09 | 0.06 |
| Limestone | 19 | 19 | 0.33 | 0.12 | 0.23 | 0.06 |
| Dolostone | 5 | 5 | 0.35 | 0.14 | 0.29 | 0.08 |

*Table B - 3* Field estimates of uniaxial compressive strength (Hoek, 2007)

| Grade | Term | Uniaxial compressive strength (MPa) | Point load index (MPa) | Field estimate of strength | Examples |
|---|---|---|---|---|---|
| R5 | Very strong | 100-250 | 4-10 | Specimen requires many blows of a geological hammer to fracture it | Amphibolite, sandstone, basalt, gabbro, gneiss, granodiorite, limestone, marble, rhyolite, tuff |
| R4 | Strong | 50-100 | 2-4 | Specimen requires more that one blow of a geological hammer to fracture it | Limestone, marble, phyllite, sandstone, schist, shale |

*Table B - 4* Values of the constant $m_i$ for intact rock, by rock group. Note that values in parenthesis are estimates (Hoek, 2007)

| Rock type | Class | Group | Texture | | | |
|---|---|---|---|---|---|---|
| | | | Coarse | Medium | Fine | Very fine |
| SEDIMENTARY | Classic | | Conglomerates (21±3) Breccias (19±5) | Sandstones 17±4 | Siltstones 7±2 Greywackes (18±3) | Claystones 4±2 Shales (6±2) Marls (7±2) |
| | Non-Classic | Carbonates | Crystalline Limestone (12±3) | Spiritic Limestone (10±2) | Micritic Limestone (9±2) | Dolomites (9±3) |
| | | Evaporites | | Gypsum 8±2 | Anhydrite 12±2 | |
| | | Organic | | | | Chalk 7±2 |
| METAMORHIC | Non Foliated | | Marble 9±3 | Homfels (19±4) Metasandstone (19±3) | Quartzites 20±3 | |
| | Slightly foliated | | Migmatite (29±3) | Amphibolites 26±6 | | |
| | Foliated | | Gneiss 28±5 | Schists 12±3 | Phyllites (7±3) | Slates 7±4 |
| IGNEOUS | Plutonic | Light | Granite 32±3 | Diorite (16±5) | | |
| | | | Granodiorite 29±3 | | | |
| | | Dark | Gabbro 27±3 Norite 20±5 | Dolerite (16±5) | | |
| | Hypabyssal | | Porphyries (20±5) | | Diabase (15±5) | Peridotite (25±5) |
| | Volcanic | Lava | | Rhyolite (25±5) Andesite 25±5 | Dacite (25±3) Basalt (25±5) | Obsidian (19±3) |

| | | | | | | |
|---|---|---|---|---|---|---|
| | | Pyroclastic | Agglomerate (19±3) | Breccia (19±5) | Tuff (13±5) | |

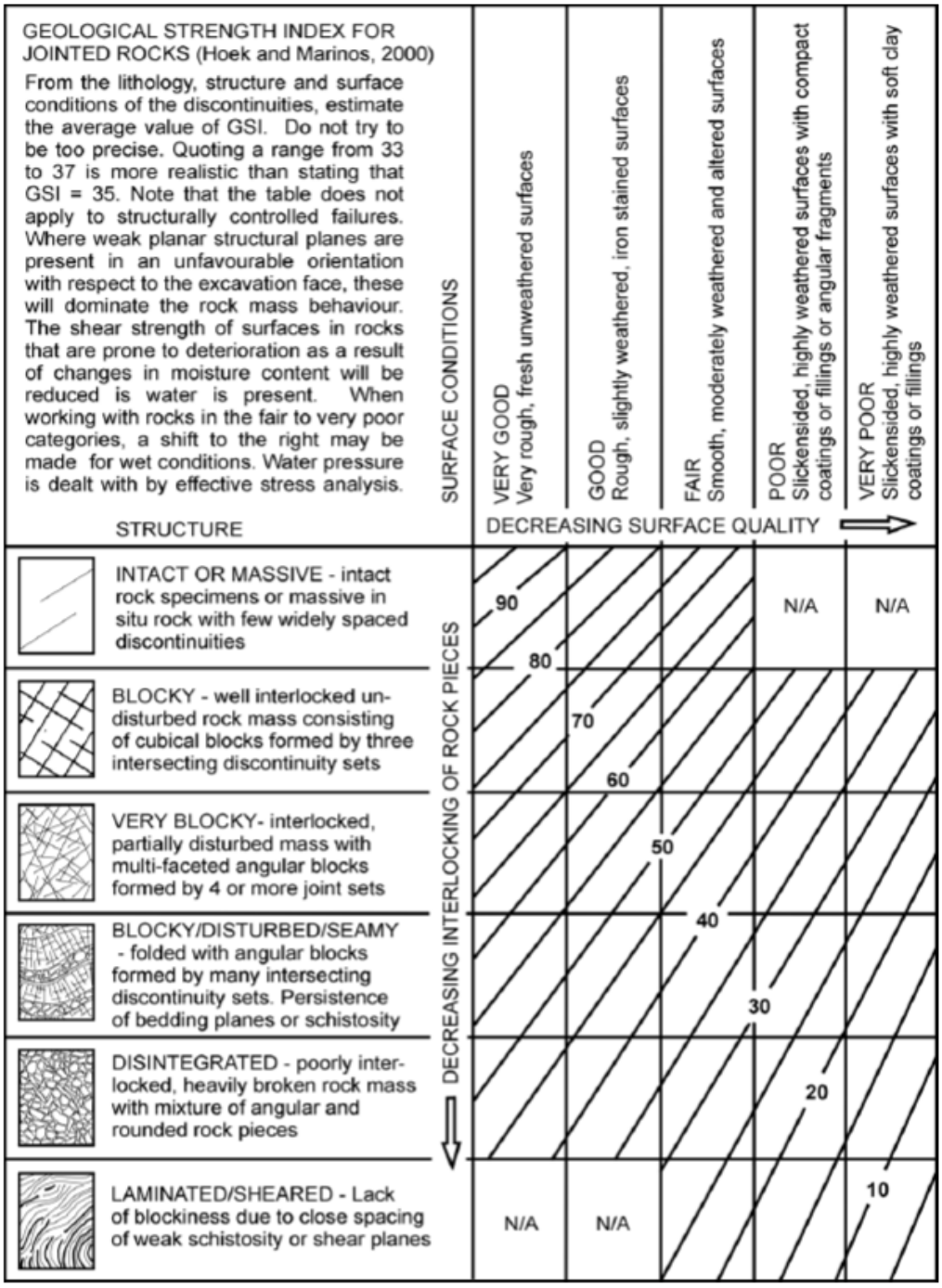


*Figure B - 1* Characterisation of blocky rock masses on the basis of interlocking and joint conditions (Hoek et al., 2013)